NV5 GEOSPATIAL

powered by QUANTUM SPATIAL
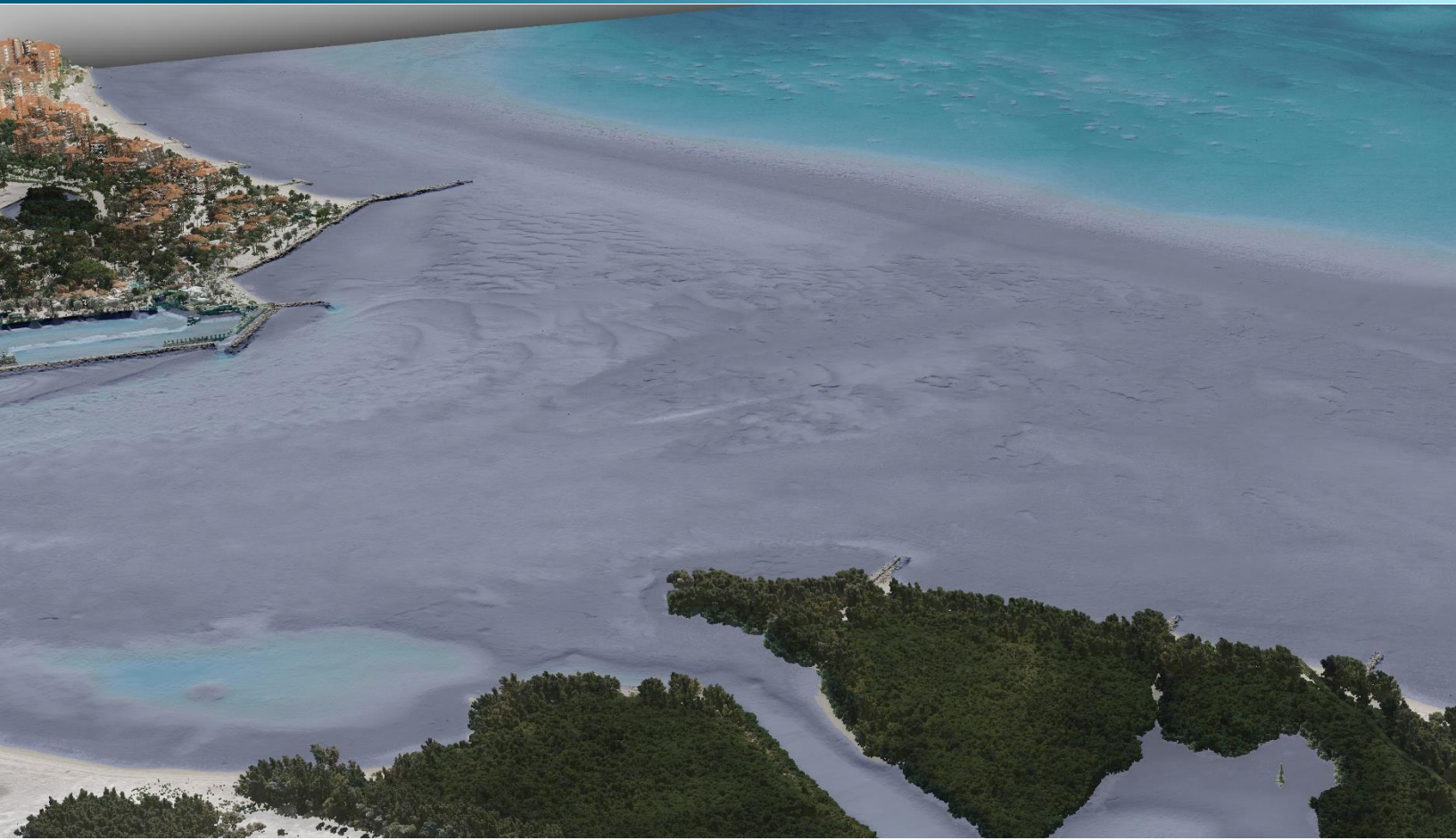
NOAA Hurricane Irma, Florida Keys

Supplemental LiDAR & Shoreline Mapping: FL-1806-TB-C

Technical Data Report, NOAA Contract: EA-133C-14-CQ-0007, Task Order 1305M218FNCNL0208

Prepared For:

NOAA; National Geodetic Survey
Gregory Stinner
1315 East West Highway
Silver Spring, MD 20910
PH: 301-713-3167 ext.133

Prepared By:

NV5 GEOSPATIAL
powered by QUANTUM SPATIAL

Quantum Spatial
1100 NE Circle Blvd, Ste. 126
Corvallis, OR 97330
PH: 301-713-3198

TABLE OF CONTENTS

Cover Photo: A view looking northeast from Virginia Key shows the topobathymetric surface of the intertidal zone near Fisher Island. This image was selected from the Hurricane Irma, Florida Keys project pilot delivery, and was created from the LiDAR bare earth model colored by elevation.

This photo taken by QSI acquisition staff shows a scenic view of the NOAA Hurricane Irma site in Florida.

Introduction

In August 2018, Quantum Spatial (QSI) was contracted by the National Oceanic and Atmospheric Administration's (NOAA) National Geodetic Survey (NGS) Remote Sensing Division (RSD) Coastal Mapping Program (CMP), to collect topobathymetric Light Detection and Ranging (Lidar) data and digital imagery in the winter of 2018 into early 2019 for the NOAA Hurricane Irma site on the coast of Florida (Contract No. EA-133C-14-CQ-0007). Data were collected to aid NOAA in assessing the topobathymetric surface of the near-shore and intertidal zones of the study area to support mapping and updating the national shoreline.

The topobathymetric LiDAR dataset was divided, processed, and delivered in five separate deliveries, while shoreline mapping products were processed in seven separate deliveries according to Geographic Cell delineations provided by NOAA. Quantum Spatial provided all Digital Imagery in one delivery package. This report provides a comprehensive summary of the delivered topobathymetric LiDAR, digital imagery dataset, and shoreline compilation products. Documented herein are contract specifications, data acquisition procedures, processing methods, and accuracy results. Acquisition dates and acreage are shown in Table 1, a complete list of contracted deliverables provided to NOAA is shown in Table 2, and the project extent is shown in Figure 1.

Table 1: Acquisition dates, acreage, and data types collected for the NOAA Hurricane Irma project

Project Site	Contracted Acres	Square Miles	Acquisition Dates	Data Type
NOAA Hurricane Irma Supplemental Mapping, Florida Keys	1,366,060	2,135	11/20/2018 - 03/23/2019	Topobathymetric LiDAR
			01/08/2019 – 05/20/2019	4 Band Digital Imagery (RGB-NIR)

Survey Area

The Hurricane Irma Supplemental project area was contracted to cover approximately 2,135 square miles in the state of Florida, along the Gulf Coast of the United States. The Hurricane Irma area of interest stretched from Miami, Florida to the Key West Islands, and covered more than 1.3 million acres of United States shoreline. Quantum Spatial conducted all LiDAR acquisition of the project area between November 20th, 2018 and March 23rd, 2019. All digital imagery acquisition was conducted between January 8th, 2019 and May 20th, 2019 by Quantum Spatial's imagery subcontractor, Geomni.
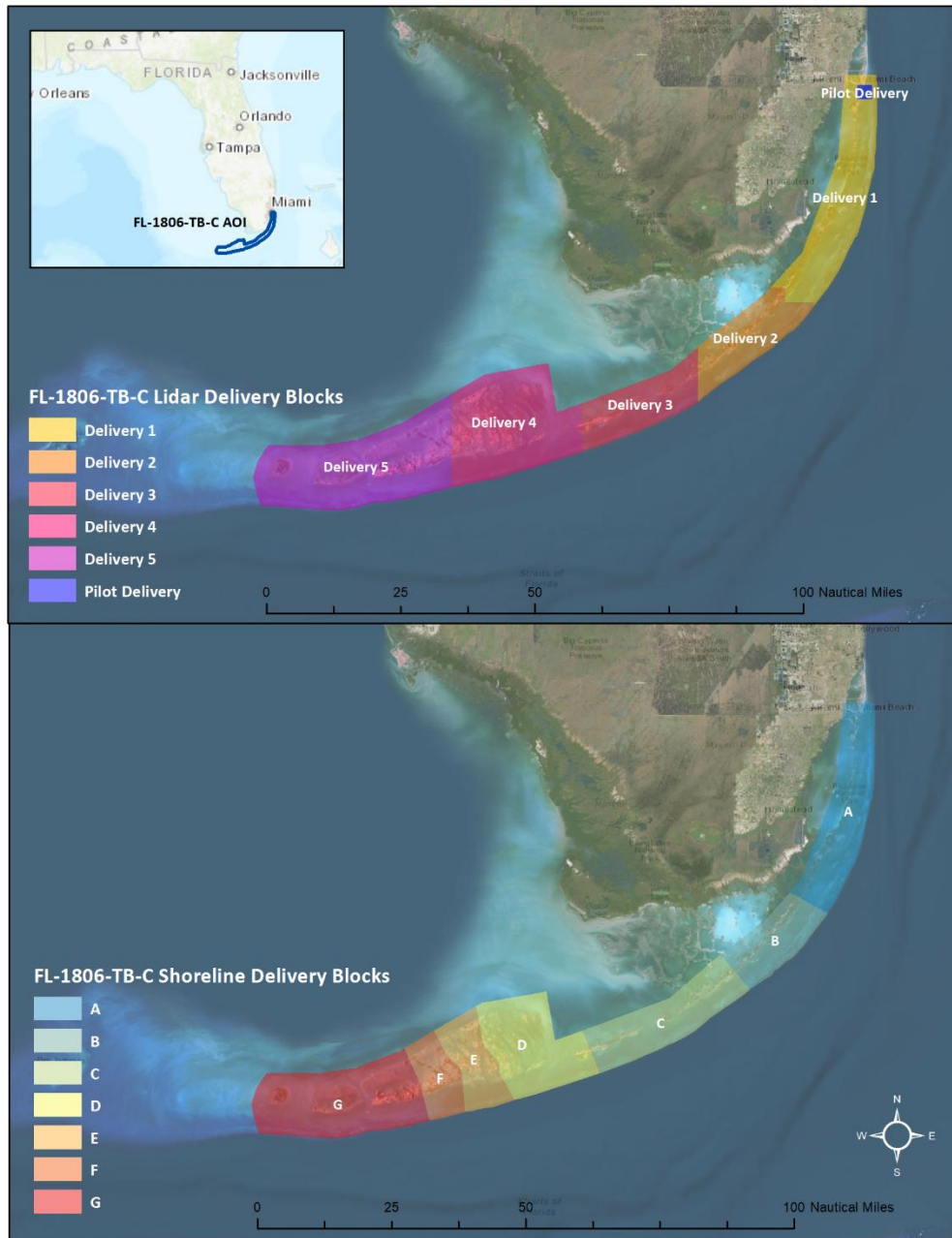

Figure 1: Location map of the NOAA Hurricane Irma site in Florida

Project Team

Quantum Spatial served as the prime contractor for the Hurricane Irma project and completed all LiDAR acquisition and processing including lidar extraction, calibration and refraction, and editing. QSI generated all Digital Elevation Models (DEM), raster layers, and LiDAR-derived void polygons from processed LiDAR data. Additionally, QSI collected all independent checkpoints to be used in assessing vertical accuracy.

A subcontractor to Quantum Spatial, Geomni, acquired all digital imagery; however, all imagery processing and supplemental ground survey collection to support the imagery production was completed by QSI's Lexington office.

NGS derived the initial shoreline files from the final delivered topobathymetric LiDAR data, and provided them to QSI for editing and attribution. All shoreline editing and deliverables were completed by Quantum Spatial's St. Petersburg office.

Deliverable Products

Table 2: Products delivered to NOAA for the NOAA Hurricane Irma, Florida Keys site

NOAA Hurricane Irma, Florida Keys Topobathymetric LiDAR Products	
Classified LAS Projection: UTM Zone 17 North **Horizontal Datum: NAD83 (2011)** **Vertical Datum: GRS80 Ellipsoidal Heights** **Units: Meters**	**DEM Projection: UTM Zone 17 North** **Horizontal Datum: NAD83 (2011)** **Vertical Datum: NAVD88 (Geoid12B)** **Units: Meters**
LiDAR	LAS v 1.4, Point Format 6 • All Classified Returns, with Depth Bias Correction and Intensity Normalization for Depth
Raster Models	1 Meter ERDAS Imagine Files (*.img) • Clipped Topobathymetric Bare Earth Digital Elevation Model (DEM) • Interpolated Topobathymetric Bare Earth Digital Elevation Model (DEM) • Topobathymetric Standard Deviation 1 Meter GeoTiffs • DZ Orthos
TPU Products	1 Meter ERDAS Imagine Files (*.img) • Total Propagated Uncertainty Raster Model (Highest Hit methodology) LAS v 1.4, Point Format 6 (*.las) • Total Propagated Uncertainty Extrabyte embedded LAS file TPU Metadata File (*.json) • Total Propagated Uncertainty values and parameters

NOAA Hurricane Irma, Florida Keys Topobathymetric LiDAR Products	
Digital Imagery	6 inch Tiled Orthomosaic GeoTiffs (*.tif) - Raw Image Frames with Socet Set SUP files and camera calibrations.
Shoreline Mapping	**Shapefiles (*.shp)** - Segmented Mean High Water Shoreline - Segmented Mean Lower Low Water Shoreline
Vectors	Shapefiles (*.shp) - Area of Interest - LiDAR Tile Index - DEM Tile Index - Bathymetric Void Shape - Flightline Shapefile - Flight Date Coverage Polygon
Reports	- Ground Survey Report (*NOAA Florida Keys Ground Survey Report_Rev3.pdf)* - Check Point Location Photos (*NOAA FK Form 76-53.zip*) - LiDAR QC Reports per Delivery (*NOAA_Florida_Keys_Delivery1_Cover_Letter.docx - NOAA_Florida_Keys_Delivery5_Cover_Letter.docx*) - Final Compiled Report of Survey - FGDC Compliant Metadata - Airborne Collection Log and Lift Extents/Coverage - Airborne Navigation and Kinematic GPS Reports - Aerotriangulation Report (*FL_1806_NOAA_Florida_Keys_Topobathy_AT_Report.doc*) - Airborne Positioning and Orientation Reports - Boresight Calibration Report - Camera Calibration Reports - EED - Photographic Flight Reports & Flightline Maps - Tabulation of Aerial Photography - Shoreline Mapping Project Completion Reports (A-G)

LiDAR Deliverables

Final topobathymetric LiDAR deliverables for the Hurricane Irma, Florida Keys project area were the final classified and tiled LiDAR returns, DZ ortho raster models, Standard Deviation raster models, topobathymetric bare earth DEMs, Total Propagated Uncertainty (TPU), and supplemental shapefiles including bathymetric void polygons and flightline swaths. QSI also provided several intermittent deliverables to NOAA in order to ensure project quality, consistency, and transparency in processing throughout the project. These additional intermittent deliverables included Quick-look LiDAR coverage maps in GeoTIFF format to display bathymetric LiDAR collection results. NOAA reviewed all QuickLook reports and approved each area for data processing or flagged each area to re-fly. RiProcess projects were also provided along with SBETs for each LiDAR collection mission to ensure that NOAA is provided with all raw topobathymetric data.

Final topobathymetric data was provided in 500 x 500 meter tiles, in five delivery blocks (Figure 1). All associated shapefiles delineating tile grids were provided to NOAA in Blocks, and as a final comprehensive tile index for the Florida Keys project area. Final LiDAR DZ Orthos were created in order to evaluate the line to line relative accuracy of the LiDAR data, and were delivered to NOAA in GeoTIFF format as well. Finally, project metadata in .xml format were delivered with all final LiDAR data and derived deliverables.

DEM Deliverables

After the final LiDAR data were accepted by NOAA, QSI processed the final classified point cloud into the contracted DEM deliverables. First, data were converted from ellipsoid heights to orthometric heights prior to DEM generation so that all final tiled DEMs include orthometric heights from Vertical Datum NAVD88, Geoid 12B, meters.

QSI provided two sets of tiled DEMs to NOAA: one with void polygons enforced so that areas lacking bathymetric bottom returns are set to "no data", and one with void areas interpolated. All DEMs were delivered in ERDAS Imagine (*.img) format with a 1 meter cell size, tiled in a 5,000 x 5,000 meter grid. Void polygons used in DEM generation were provided in addition to a confidence layer. The confidence layer reports the standard deviation (in meters) of all ground and bathymetric bottom return points within each 1 meter cell, provided in ERDAS Imagine (*.img) format with a 1 meter pixel resolution, tiled in 500 x 500 meter grid.

Imagery Deliverables

QSI provided NOAA with all acquired image frames to be viewed in both stereo as well as mosaic format. All appropriate imagery orientation and calibration information was provided along with image frames, including Socet Set SUP files and a center point shapefile. Metadata were delivered in .xml format for both stereo imagery and orthomosaics.

The collected 4-band (RGB/NIR) digital imagery was processed with 3000 x 3000 meter tile delineation, and mosaicked in GeoTIFF format. In total, 964 final orthomosaics were provided in the deliverable coordinate system: Projection: UTM Zone 17 North, Horizontal Datum: NAD83 (2011) epoch 2010.00, meters. For detailed processing information, please reference documentation provided with the imagery delivery, which includes: Aerotriangulation Report, Airborne Positioning and Orientation Report, Boresight Calibration Report, Camera Calibration Reports, EED, Flightline Maps, Ground Control Report, Photographic Flight Reports, and Tabulation of Aerial Photography.

Shoreline Deliverables

NOAA supplied QSI with LiDAR derived Mean High Water (MWH) and Mean Lower-Low Water (MLLW) shorelines to be segmented, edited, and attributed. In addition, QSI was responsible for compiling any shoreline features that were unable to be extracted from the LiDAR. These features were compiled photogrammetrically using stereo imagery flown specifically for this project.

QSI received and mapped the shoreline from NOAA in seven processing blocks between Miami Beach and Mooney Harbor Key, Florida. Each processing block was identified with a Geographic Cell number and included all bays, inlets, and islands within 2000 feet of the coastline.

Figure 2: A scenic photo of the Florida Coastline taken by the Quantum Spatial Field Operations Team

This photo shows a view of the Florida Keys project area taken from QSI's Cessna Caravan.

Sensor Selection: the Riegl VQ-880-G Series

The Riegl VQ-880-G series were selected as the hydrographic airborne laser scanners for the NOAA Hurricane Irma project based on fulfillment of several considerations deemed necessary for effective mapping of the project site. A higher combined pulse rate (up to 550 kHz), higher scanning speed, small laser footprint, and wide field of view allow for seamless collection of high-resolution data of both topographic and bathymetric surfaces. A short laser pulse length allows for discrimination of underwater surface expression in shallow water. Sensor specifications and settings for the NOAA Hurricane Irma acquisition are displayed in Table 3.

Planning

In preparation for data collection, QSI reviewed the project area and developed a specialized flight plan to ensure complete coverage of the NOAA Hurricane Irma LiDAR study area at the target point density of ≥2.0 points/m^2. Acquisition parameters including orientation relative to terrain, flight altitude, pulse rate, scan angle, and ground speed were adapted to optimize flight paths and flight times while meeting all contract specifications.

QSI's acquisition team considered several environmental conditions during the planning stage in order to target the best possible windows for capturing bathymetric bottom returns. Water clarity was monitored using several water quality stations, in addition to handheld Hach turbidity meters operated by QSI ground operations professionals (Figure 3).

Figure 3: Hach Turbidity Meter

Flights over shoreline areas were planned during optimal conditions with low wind and wave conditions whenever possible, and within 20% of the Mean Range of tide around Mean Lower Low Water (MLLW) as contractually specified. Quantum Spatial acquisition teams carefully monitored NOAA tide stations at Biscayne Bay (8723214), Florida Bay (8723970), and Key West (8724580) to ensure acquisition requirements were met or exceeded.[1] Utilized stations are indicated with a blue dot in Figure 4 below. Quantum Spatial acquisition managers oversaw all logistical considerations including private property access and coordination of NOTAMs prior to flights.
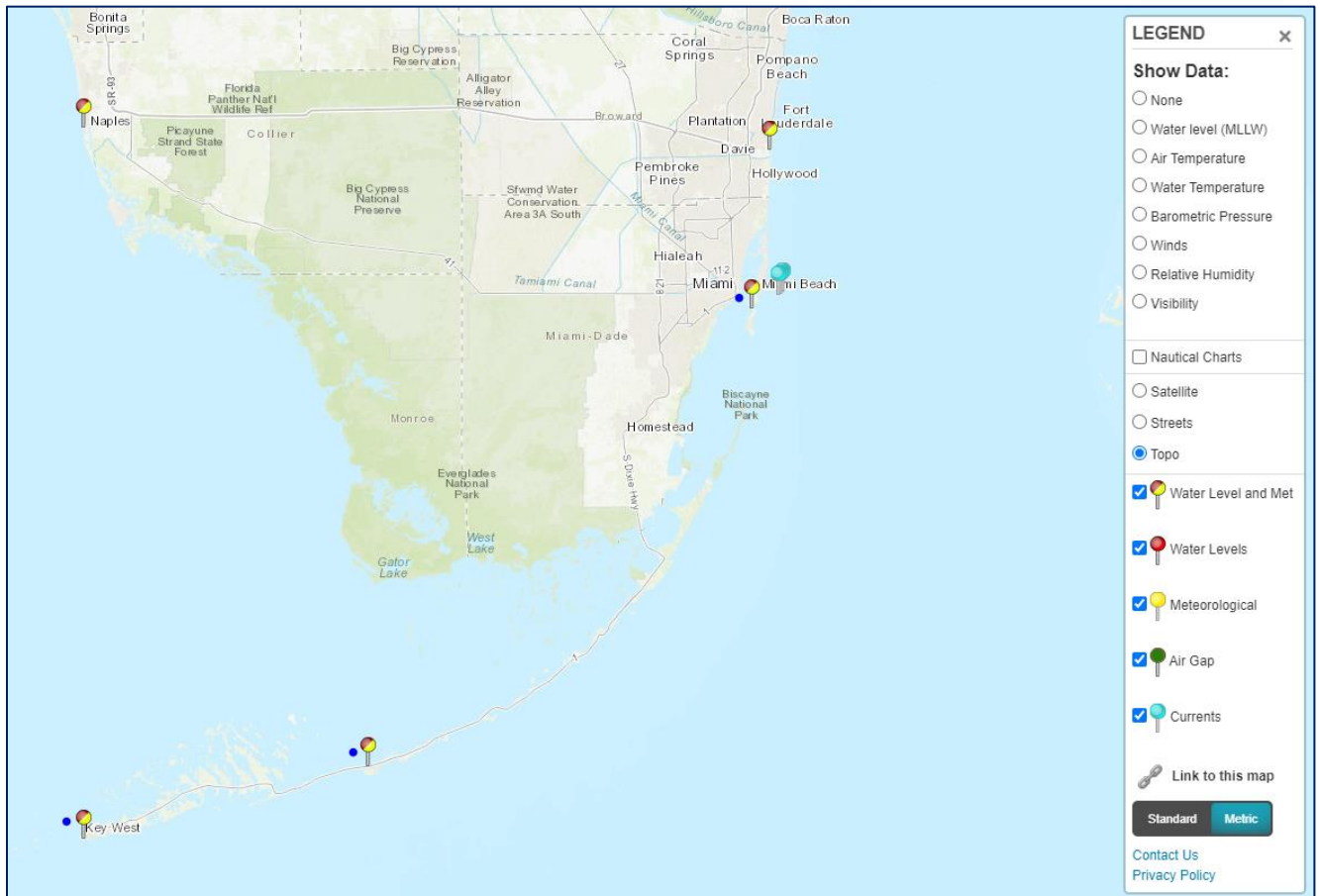
Figure 4: NOAA Tide Station Map

---

[1] NOAA Tides and Currents: https://tidesandcurrents.noaa.gov/map/

Airborne LiDAR Survey

The LiDAR survey was accomplished using a Riegl VQ-880-G green laser system (or equivalent) mounted in a Cessna Caravan. The Riegl VQ-880-G uses a green wavelength ($ʎ$=532 nm) laser that is capable of collecting high resolution vegetation and topography data, as well as penetrating the water surface with minimal spectral absorption by water. The Riegl VQ-880-G also contains an integrated NIR laser ($ʎ$=1064 nm) that aids in water surface modeling for refraction purposes. The recorded waveform enables range measurements for all discernible targets for a given pulse. It is not uncommon for some types of surfaces (e.g., dense vegetation or water) to return fewer pulses to the LiDAR sensor than the laser originally emitted. The discrepancy between first return and overall delivered density will vary depending on terrain, land cover, and the prevalence of water bodies. All discernible laser returns were processed for the output dataset. Table 3 summarizes the settings used to yield an average first return pulse density of $\geq$ 2 pulses/m^2 over the NOAA Hurricane Irma project area.

Table 3: LiDAR specifications and survey settings

LiDAR Survey Settings & Specifications		
Acquisition Dates	11/20/2018 - 03/23/2019	11/20/2018 - 03/23/2019
Aircraft Used	Cessna Caravan	Cessna Caravan
Sensor	Riegl	Riegl
Laser	VQ-880-G, GII, or GH	VQ-880-G-IR
Maximum Returns	15 (LAS 1.4 Format)	15 (LAS 1.4 Format)
Resolution/Density	To exceed 2 pulses/m^2	To exceed 2 pulses/m^2
Nominal Pulse Spacing	0.71 m	0.71 m
Survey Altitude (AGL)	400 m	400 m
Survey speed	140 knots	140 knots
Field of View	40°	40°
Mirror Scan Rate	80 revolutions per second	Uniform Point Spacing
Target Pulse Rate	245 kHz	245 kHz
Pulse Length	1.5 ns	3 ns
Laser Pulse Footprint Diameter	28 cm	8 cm
Central Wavelength	532 nm	1064 nm
Pulse Mode	MTA (multiple times around)	MTA (multiple times around)
Beam Divergence	0.7 mrad	0.2 mrad
Swath Width	291 m	291 m
Swath Overlap	30%	30%
Intensity	16-bit	16-bit
Accuracy	RMSE$_Z$ $\leq$ 15 cm	RMSE$_Z$ $\leq$ 15 cm

All areas were surveyed with an opposing flight line side-lap of ≥30% (≥60% overlap) in order to reduce laser shadowing and increase surface laser painting. To accurately solve for laser point position (geographic coordinates x, y and z), the positional coordinates of the airborne sensor and the attitude of the aircraft were recorded continuously throughout the LiDAR data collection mission. Position of the aircraft was measured twice per second (2 Hz) by an onboard differential GPS unit, and aircraft attitude

was measured 200 times per second (200 Hz) as pitch, roll and yaw (heading) from an onboard inertial measurement unit (IMU). To allow for post-processing correction and calibration, aircraft and sensor position and attitude data are indexed by GPS time.

Airborne Collection Logs & Coverage Reports

QSI provided daily airborne collection logs to NOAA throughout the acquisition process in the form of a daily blog and acquisition tracker update on QSI's tracking platform InSITE. Information included in each report detail the collection date, tide window and conditions, lines collected, coverage, and operator notes (Figure 5).
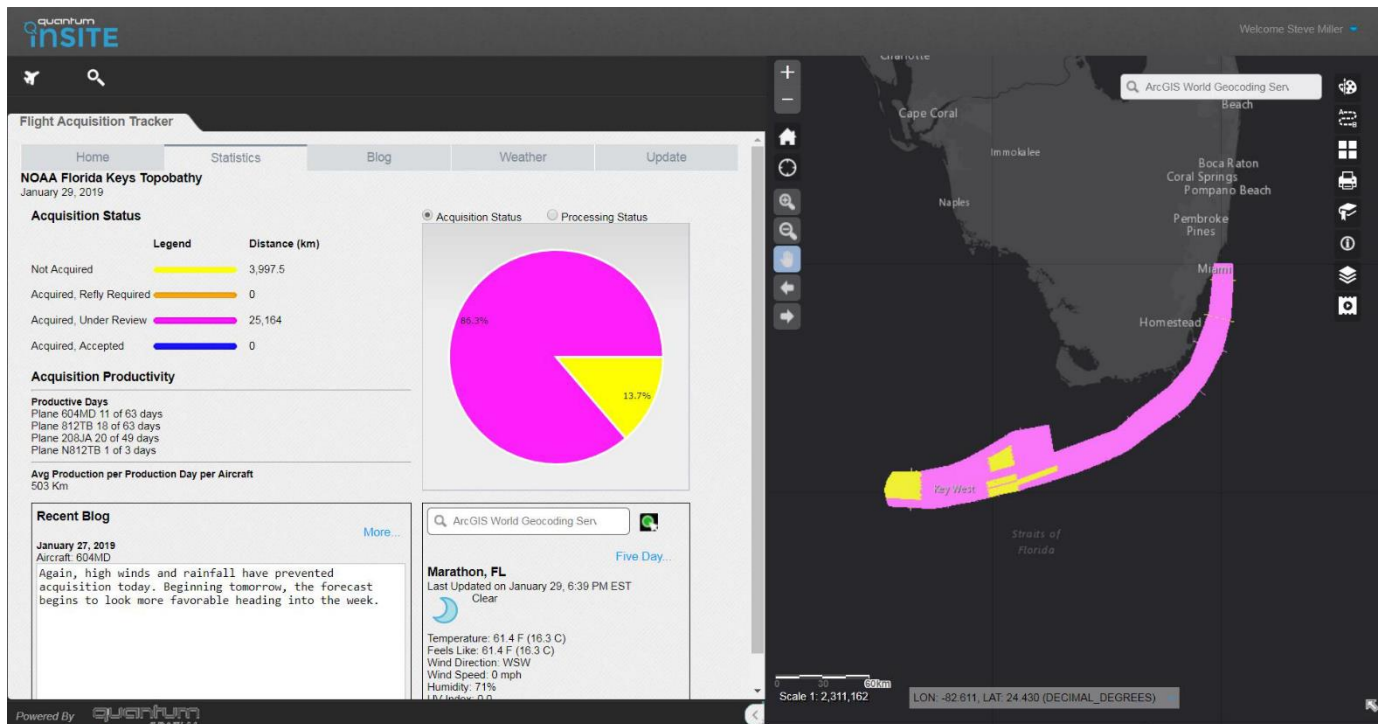

Figure 5: Airborne acquisition status reporting via inSITE

Ground Control

Ground control surveys were conducted to support the airborne acquisition. Ground control data were used to geospatially correct the aircraft positional coordinate data and to perform quality assurance checks on final LiDAR data.

Base Stations

QSI utilized nine permanent RTN stations for the NOAA Hurricane Irma project. Three base stations were from the VRS-Now network and six were from the FPRN. The position, precision, and network of each base station have been provided in Table 4. Record positions were held for all base stations.

QSI triangulated static Global Navigation Satellite System (GNSS) data (1 Hz recording frequency) from each base station with nearby Continuously Operating Reference Stations (CORS) using the Online Positioning User Service (OPUS[2]) to ensure alignment with the National Spatial Reference System (NSRS), updating record positions as necessary. Multiple independent sessions over the same monument were processed to confirm antenna height measurements and to refine position accuracy. The five NGS CORS utilized during OPUS Project processing are listed in Table 5.

Table 4: Permanent Real-Time Network (RTN) stations utilized for the NOAA Hurricane Irma acquisition. Coordinates are on the NAD83 (2011) datum, epoch 2010.00. Units are in meters.

Station ID	Latitude	Longitude	Ellipsoid (meters)	Network	Held?
FLKW	24° 33' 13.26664"	-81° 45' 15.39914"	-10.257	FPRN	YES
FLKW*	24° 39' 33.67173"	-81° 31' 20.54518"	-11.211	VRSNOW	YES
FLMA	24° 43' 06.59490"	-81° 04' 06.74239"	-11.711	FPRN	YES
FLMB	25° 46' 57.83786"	-80° 08' 14.16764"	-15.518	FPRN	YES
FLMK	24° 43' 33.36203"	-81° 02' 56.70329"	-13.903	FPRN	YES
FLPK	24° 57' 47.22531"	-80° 34' 05.39838"	-13.201	FPRN	YES
FLUM	25° 43' 54.86870"	-80° 09' 48.52710"	-5.285	VRSNOW	YES
HMST	25° 28' 13.58298"	-80° 29' 19.63111"	-16.134	VRSNOW	YES
HOME	25° 30' 03.79565"	-80° 33' 00.43217"	-19.134	FPRN	YES

* Trimble VRS-Now and FPRN independently include a station named FLKW. It is not a duplicate.

Table 5: NGS CORS utilized with OPUS Project. Published NAD83(2011) coordinates were held and can be retrieved from http://www.ngs.noaa.gov/CORS/.

CORS used in OPUS Project		
FLBN	FLF1	GACR
GNVL	ZMA1	

---

[2] OPUS is a free service provided by the National Geodetic Survey to process corrected monument positions. http://www.ngs.noaa.gov/OPUS.

Network Accuracy

Base station coordinates were established according to the national standard for geodetic control networks, as specified in the Federal Geographic Data Committee (FGDC) Geospatial Positioning Accuracy Standards for geodetic networks.[3] This standard provides guidelines for classification of monument quality at the 95% confidence interval as a basis for comparing the quality of one control network to another. The monument rating for this project is shown in Table 6.

Table 6: Federal Geographic Data Committee monument rating for network accuracy

Direction	Rating
1.96 * St Dev $_{NE}$:	0.020 m
1.96 * St Dev $_z$:	0.050 m

Ground Survey Points (GSPs)

Ground survey points were collected using real time kinematic (RTK), post-processed kinematic (PPK), and fast-static (FS) survey techniques. For RTK surveys, a roving receiver receives corrections from a nearby base station or Real-Time Network (RTN) via radio or cellular network, enabling rapid collection of points with relative errors less than 1.5 cm horizontal and 2.0 cm vertical. PPK and FS surveys compute these corrections during post-processing to achieve comparable accuracy. RTK and PPK surveys record data while stationary for at least five seconds, calculating the position using at least three one-second epochs. FS surveys record observations for up to fifteen minutes on each GSP in order to support longer baselines. All GSP measurements were made during periods with a Position Dilution of Precision (PDOP) of ≤ 3.0 with at least six satellites in view of the stationary and roving receivers. See Table 7 for QSI ground survey equipment information.

GSPs were collected in areas where good satellite visibility was achieved on paved roads and other hard surfaces such as gravel or packed dirt roads. GSP measurements were not taken on highly reflective surfaces such as center line stripes or lane markings on roads due to the increased noise seen in the laser returns over these surfaces. GSPs were collected within as many flightlines as possible; however the distribution of GSPs depended on ground access constraints and monument locations and may not be equitably distributed throughout the study area (Figure 6).

Table 7: Trimble equipment identification

Receiver Model	Antenna	OPUS Antenna ID	Serial Numbers	Use
Trimble R8 Model 2	Integrated Antenna	TRMR8_GNSS	0649, 8595	Rover, Static
Trimble R8 Model 3	Integrated Antenna	TRMR8_GNSS3	9860	Rover

---

[3] Federal Geographic Data Committee, Geospatial Positioning Accuracy Standards (FGDC-STD-007.2-1998). Part 2: Standards for Geodetic Networks, Table 2.1, page 2-3. http://www.fgdc.gov/standards/projects/FGDC-standards-projects/accuracy/part2/chapter2

Land Cover Class

In addition to ground survey points, land cover class check points were collected throughout the study area to evaluate vertical accuracy. Vertical accuracy statistics were calculated for all land cover types to assess confidence in the LiDAR derived ground models across land cover classes (Table 8, see LiDAR Accuracy Assessments, page 26).

Table 8: Land Cover Types and Descriptions

Land cover type	Land cover code	Example	Description	Accuracy Type
Shrub Land	SHRUB, SH		Maintained or low growth herbaceous grasslands	VVA
Tall Grass	TALL_GRASS, TG		Herbaceous grasslands in advanced stages of growth	VVA
Forest	FOREST, FR, FO		Forested areas	VVA

Land cover type	Land cover code	Example	Description	Accuracy Type
Bare Earth	BARE, BE		Areas of bare earth surface	NVA
Urban	URBAN, UA		Areas dominated by urban development, including parks	NVA
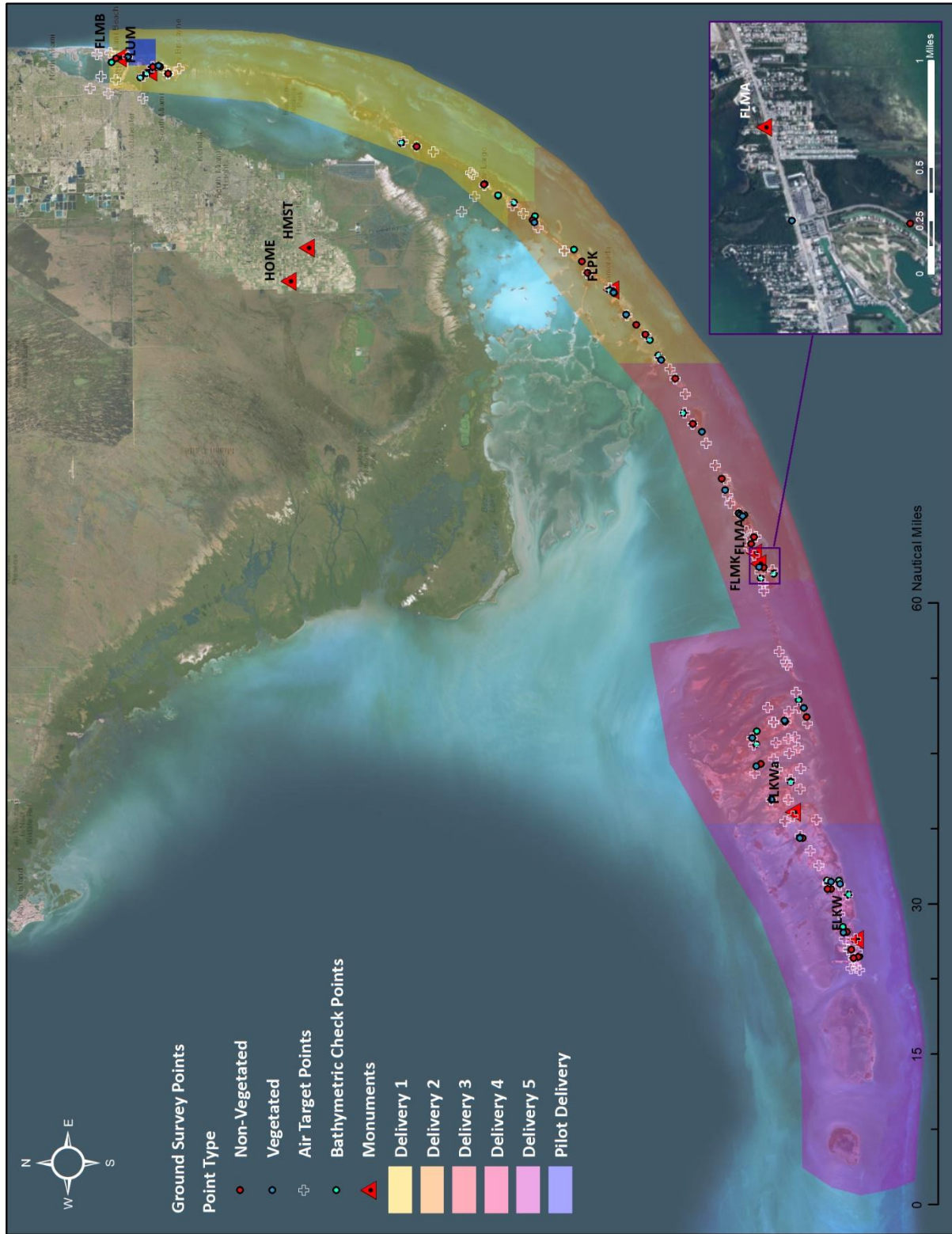
Figure 6: Ground survey location map

Digital Imagery

Survey Settings

Aerial imagery was collected by Geomni at a nominal ground sample distance of 0.33 meters using the DMCII 230-526 camera with a 92.00 mm lens. The DMCII is a large format digital aerial camera manufactured by Intergraph. The system is gyro-stabilized with forward motion compensation and simultaneously collects panchromatic and multispectral (RGB, NIR) imagery through eight individual camera modules. Raw image data radiometrics were processed from the solid-state disc (SSD) to compensate for the effects of vignetting, aperture, and other radiometric factors. The intermediate images were then geometrically corrected for lens distortion and tilt, and output in high resolution panchromatic color (RGB) and near infrared.

All imagery was acquired using >60% forward overlap and >30% side overlap, sun angles >20 or >25 degrees (depending on the date of acquisition) and was coordinated with low tide. Acquisition settings particular to the Hurricane Irma, Florida Keys project were provided to NOAA along with QSI's imagery delivery.

Table 9: Camera manufacturer's specifications

DMC II	
Focal Length	92.00 mm
Data Format	RGB NIR
Pixel Size	5.6 µm
Image Size	15,552 x 14,144 pixels
FOV	53.8° cross track x 49.5° along track

Aerial Targets

All ground survey work in support of imagery production was completed by QSI's Lexington office. A detailed report of survey for imagery was provided to NOAA in previous delivery packages, and can be referenced in Appendix B.
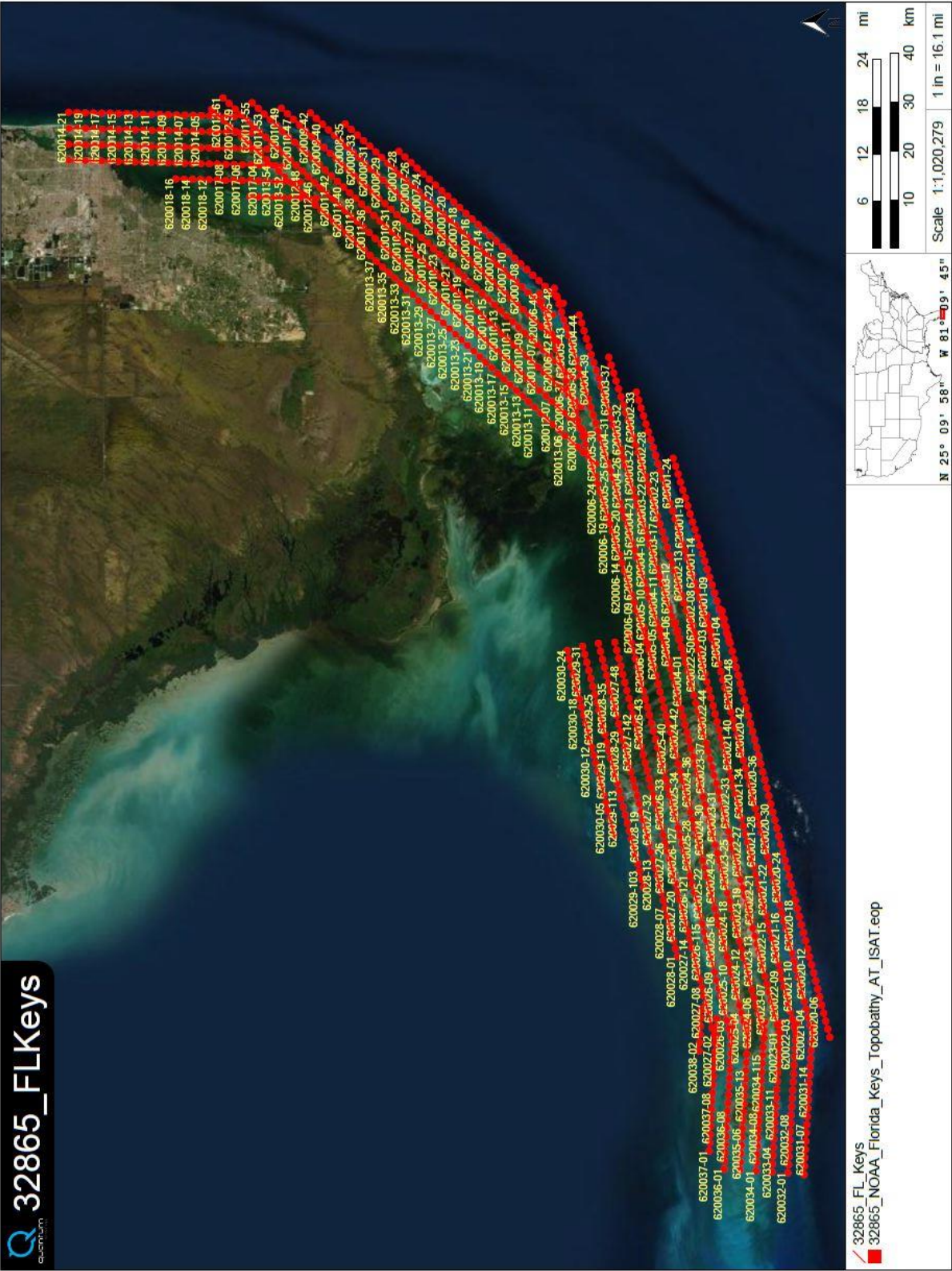
Figure 7: Map showing imagery acquisition lines

Technical Data Report – Hurricane Irma Topobathymetric-Shoreline Mapping

A cross section view of the Florida Keys classified point cloud showing bathymetric bottom returns in yellow.
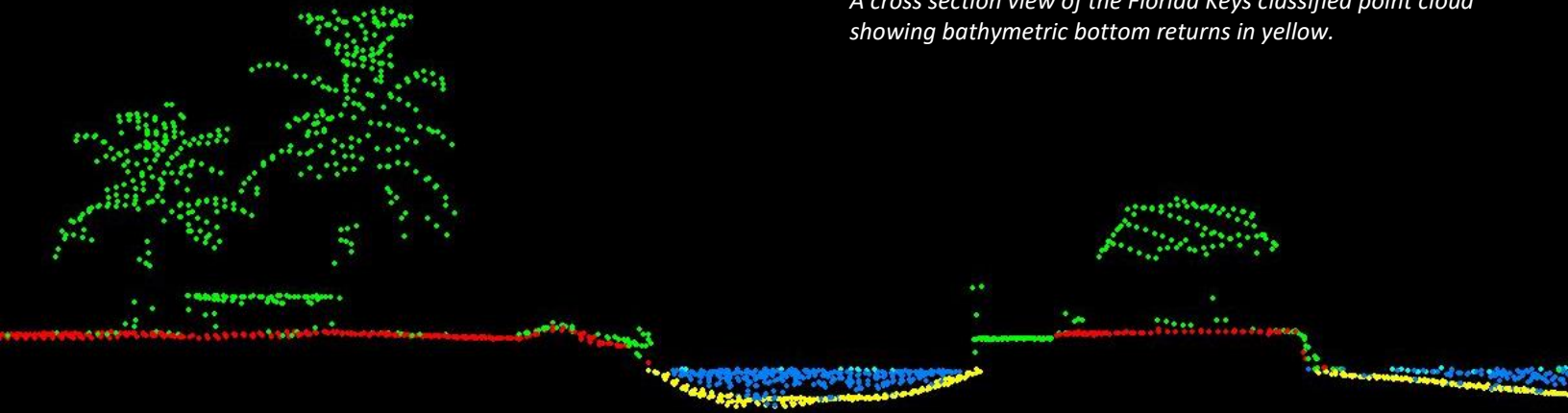
LiDAR Data Calibration

Upon completion of data acquisition, QSI processing staff initiated a suite of automated and manual techniques to process the data into a geo-referenced point cloud ready for refraction processing and classification routines. Solutions for Smoothed Best Estimates of Trajectory (SBET) were processed using Applanix POSPac 8.3 SP3 using their Trimble® CenterPoint™ Post-Processed Real-Time Extended (PP-RTX) solution. This process utilizes the GPS and IMU data recorded onboard the aircraft, real-time data from Trimble's global reference station infrastructure, and advanced positioning and compression algorithms to calculate a highly accurate SBET for each mission.

Laser return point position computations were completed in Riegl's SDCImport and RiWorld software using the SBET and raw range information. After extracting the laser swaths, swath-to-swath geometric corrections were found using least square fit regression of matching tie plane objects in RiProcess. Individual lifts were adjusted to match vertical ground control points where available, and then integrated with corresponding overlapping lifts. Any remaining swath-swath discrepancies were further resolved using Terrasolid's TerraMatch application.

Bathymetric Refraction

The water surface models used for refraction were generated using elevation information from the point cloud. Where possible, points from the NIR channel were preferred due to the clean characteristics of water surface returns from that wavelength. However, because the NIR and green channels are not spatially and temporally coincident in the VQ-880-G system, where substantial wave action was present the green channels were used instead. Advanced classification routines were employed to ensure above-surface spray and below-surface backscatter points were not included in the model. Points were automatically classified, passed through filters appropriate to surface characteristics, and then manually edited to obtain the most accurate representation of the water surface. Models were created for each flight line to accommodate water level changes due to tide or other temporal factors.

Page 18

The refraction correction was applied to submerged points using QSI's proprietary software Las Monkey. Points were flagged to refract based on their position relative to the triangulated irregular network model representing the water surface. Using the information from the trajectory and water surface model, each point was spatially corrected for refraction through the water column based on the angle of incidence of the laser to the model. The resulting point cloud was classified into its final scheme using both manual and automated techniques (Table 10).

Table 10: ASPRS LAS classification standards applied to the NOAA Hurricane Irma dataset

Classification Number	Classification Name	Classification Description
1	Unclassified	Processed, but unclassified
2	Ground	Bare-earth ground
7	Noise	Noise (low or high; manually identified)
40	Bathymetric Bottom	Bathymetric point (e.g., seafloor or riverbed; also known as submerged topography)
41	Water Surface	Water's surface (sea/river/lake surface from topographic-bathymetric LiDAR
42	Derived Water Surface	Synthetic water surface location used in computing refraction at water surface
43	Submerged Feature	Submerged object, not otherwise specified (e.g., wreck, rock, submerged piling)
44	S-57 Object	International Hydrographic Organization (IHO) S-57 object, not otherwise specified
45	Water Column	Refracted returns not determined to be water surface or bathymetric bottom
46	Overlap Bathymetric Bottom	Denotes bathymetric bottom temporal changes from varying lifts, not utilized in the bathymetric point class
71	Adjacent Lift Unclassified	Adjacent lift Unclassified associated with areas of overlap bathy bottom where temporal bathymetric differences are present
72	Adjacent Lift Ground	Adjacent lift Ground associated with areas of overlap bathy bottom where temporal bathymetric differences are present
81	Adjacent Lift Water Surface	Adjacent lift Water Surface associated with areas of overlap bathy bottom where temporal bathymetric differences are present
85	Adjacent Lift Water Column	Adjacent lift Water Column associated with areas of overlap bathy bottom where temporal bathymetric differences are present
1-Overlap	Edge Clip	Unclassified points flagged as withheld. These are primarily "edge" points from the higher scan angle being removed
139	Withheld Tail Clip	These are points from the start/end of lines overlapping in adjoining lifts where flight data is not consistent or necessary to create coverage

Original SOW classification scheme	Delivered in LAS files
Additional classification codes	Delivered in LAS files
Original SOW classification code not used	Not delivered in LAS files
Deleted points	Not delivered in LAS files

Table 11: Lidar Processing Workflow

LiDAR Processing Step	Software Used
GNSS/IMU processing to create smoothed best estimate of trajectory using PP-RTX technology.	Applanix POSPac v.8.3 Service Pack 3
Extract raw laser data and calculate laser point positions. Calculation combines raw ranging information, processed SBET, automated determination of MTA (Multiple-Time-Around) zone, and coordinate system information to extract and georeference each laser return.	Riegl SDCImport v.2.3 Riegl RiWorld v.5.1
Sensor boresight. Per-lift geometric adjustments based on least-squares adjustment of feature matched tie planes.	Riegl RiProcess v.1.8
Apply refraction correction and depth bias correction to subsurface returns.	LAS Monkey v.2.0 (QSI)
Import raw laser points into manageable blocks to perform manual relative accuracy calibration and filter erroneous points. Classify ground points for individual flight lines.	TerraScan v.19
Using ground classified points per flight line, perform automated line-to-line calibrations for system attitude parameters (pitch, roll, and heading). Match data to vertical control points. Assess relative accuracies between overlapping lifts and relative within each lift and swath.	TerraMatch v.19 Las Product Creator v.3.4 (QSI)
Classify resulting data to ground and other client-designated classifications using manual and automated processes (Table 10**Error! Reference source ot found.**). Assess statistical absolute accuracy via direct comparisons of ground classified points and the Bare Earth DEM to ground control survey data.	TerraScan v.19 TerraModeler v.19
Convert data to orthometric elevations by applying a geoid correction for DEM creation. Generate bare earth models as triangulated surfaces. Export all surface models in ERDAS Imagine (.img) format at a 1 meter pixel resolution.	TerraScan v.19 ArcMap v. 10.3.1 LasProjector v.1.2 (QSI) LPD v 3.0.28 (QSI)
Export intensity images layered under DZ Orthos as GeoTIFFs at a 1 meter pixel resolution.	ArcMap v.10.3.1 Las Product Creator v.3.4 (QSI)
Export standard deviation of ground, bathymetric bottom, and submerged objects in ERDAS Imagine (.img) format at a 1 meter pixel resolution	LAS Tools

Topobathymetric DEMs

Bathymetric bottom returns can be limited by depth, water clarity, and bottom surface reflectivity. Water clarity and turbidity affects the depth penetration capability of the green wavelength laser with returning laser energy diminishing by scattering throughout the water column. Additionally, the bottom surface must be reflective enough to return remaining laser energy back to the sensor at a detectable level. Although the predicted depth penetration range of the Riegl VQ-880-G sensor is 1.5 Secchi depths on brightly reflective surfaces, it is expected for turbid or non-reflective areas to have 0 or no returns.

As a result, creating digital elevation models (DEMs) presents a challenge with respect to interpolation of areas with no returns. Traditional DEMs are "unclipped", meaning areas lacking ground returns are interpolated from neighboring ground returns, with the assumption that the interpolation is close to reality. In bathymetric modeling, these assumptions are prone to error because a lack of bathymetric returns can indicate a change in elevation that the laser can no longer map due to increased depths. The resulting void areas may suggest greater depths, rather than similar elevations from neighboring bathymetric bottom returns. Therefore, QSI created a polygon of bathymetric voids to delineate areas outside of successfully mapped bathymetry. This shapefile was used to control the extent of the delivered clipped topobathymetric model and to avoid false triangulation across areas in the water with no returns. Insufficiently mapped areas were identified by triangulating bathymetric bottom points with an edge length maximum of 4.56 meters. This ensured all areas of no returns (> 9 m^2), were identified as bathymetric data voids.
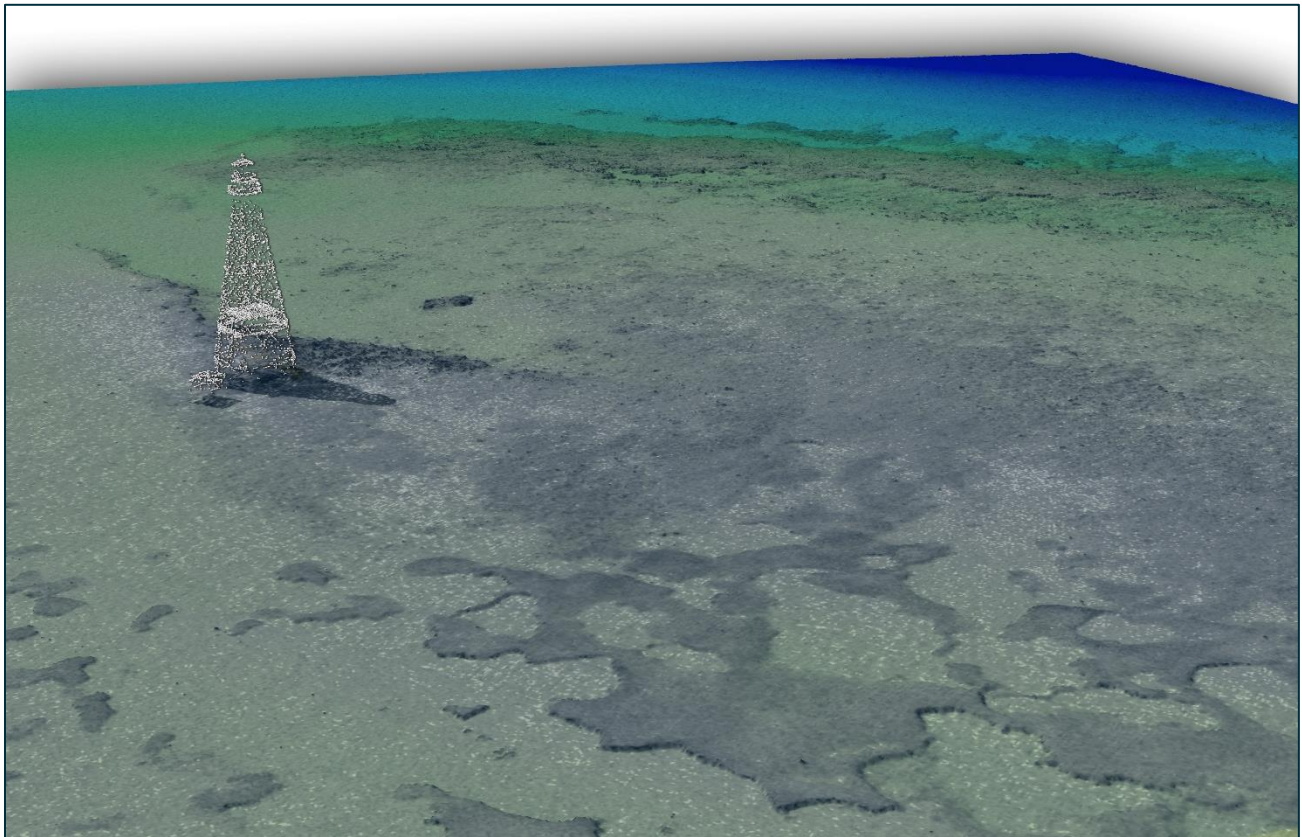
Figure 8: Traditional interpolated topobathymetric bare earth digital elevation model colored by elevation. The above-ground points display a lighthouse captured in the Florida Keys dataset, colored by intensity.

Normalized Seabed Reflectance

The lidar echo return signal has a recorded amplitude associated for each point and is expressed in LAS files as an Intensity record. Laser return intensity is generally a unitless measure of discrete return signal strength, stored as a 16-bit integer value from 0 to 65,535. Intensity values roughly correspond to the reflectivity of the surface, which is a function of surface material composition. The magnitude of intensity values can vary across similar surfaces due to variability in atmospherics, water clarity, range, submerged depth, and the angle of incidence on the object. The result is line to line inconsistency and streaking in the images that can reduce the utility of these data for analytics. The Intensity value in the LAS file has been updated with corrected values that have normalized the effects of the variables described above.

When a laser pulse enters the water column, the return signal fades exponentially with depth, and the rate of decay depends on the water properties like turbidity and composition. This exponential darkening can be corrected after determining the rate of decay by comparing similar substrates across multiple flightlines and varying depths. This dataset has been corrected for depth attenuation but is still subject to localized changes of water properties within the water column across a water body. Best efforts have been made to match line to line variability based on the overall histogram of intensity values for each line.

Total Propagated Uncertainty

To have topobathymetric lidar data support NOAA's nautical charting updates, the sum of all the potential sources of uncertainty surrounding positioning measurements are calculated to provide an estimate of the total propagated uncertainty (TPU). This is a necessary component for updating depths with and accurate positioning. NOAA has developed a tool, cBlue, for calculating these uncertainty estimates[4]. The cBlue tool estimates subaerial components of the laser pulse's travel path utilizing information from associated flight trajectory (Smooth Best Estimate of Trajectory), lidar sensor model. Calculating the subaqueous components of a bathymetric laser pulse utilizes Monte Carlo ray tracing simulations that take in account environmental factors of wind speed, water clarity, and depth. The maximum cumulative uncertainty for the VDatum region is also included in TPU estimates. These subaerial and subaqueous estimates of uncertainty are combined to produce a total propagated horizontal and vertical uncertainty.

The outputs of the cBlue tool (LAS and *.json metadata files) are delivered along with a derived raster model of the total propagated vertical uncertainty value. The raster model is a 1 square meter resolution grid of the highest associated TPU value calculated from the bathymetric bottom or submerged object classified points in each cell.

---

[4] NOAA cBlue: https://noaa-rsd.github.io/cBLUE.github.io/index.html
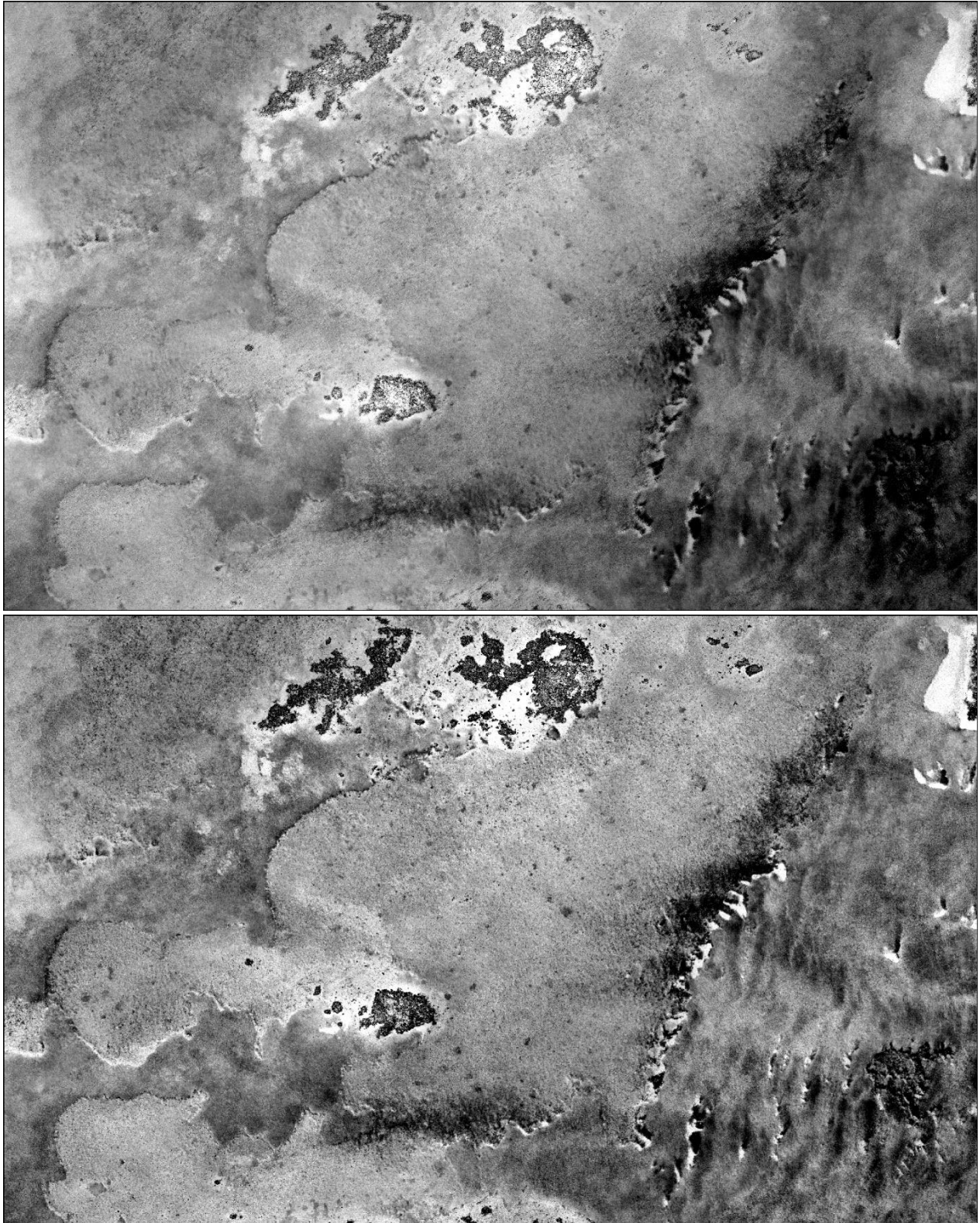
Figure 9: Top is an intensity image not corrected for depth attenuation. The tops of reef patches (lower reflectivity) appear brighter than surrounding bottom (higher reflectivity) due to shallower depths. Bottom is the same intensity image corrected for depth; the tops of reef patches are darker and consistent with the rest of the reef patch.

This lidar cross section shows a Lighthouse in the Florida Keys point cloud, colored by laser pulse echo.

Only Echo — green
First of Many — red
Intermediate — yellow
Last of Many — cyan
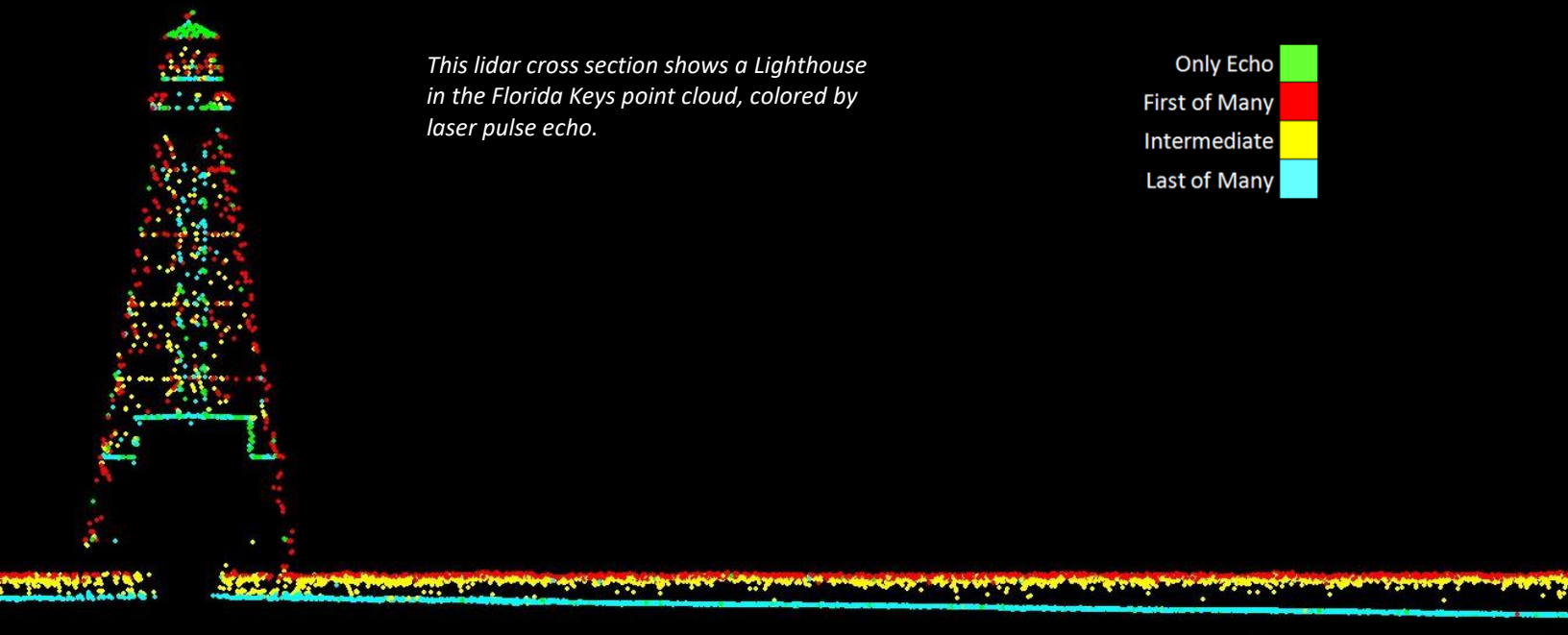
LiDAR Point Density

First Return Point Density

The acquisition parameters were designed to acquire an average first-return density of 2 points/m^2. First return density describes the density of pulses emitted from the laser that return at least one echo to the system. Multiple returns from a single pulse were not considered in first return density analysis. Some types of surfaces (e.g., breaks in terrain, water and steep slopes) may have returned fewer pulses than originally emitted by the laser.

First returns typically reflect off the highest feature on the landscape within the footprint of the pulse. In forested or urban areas the highest feature could be a tree, building or power line, while in areas of unobstructed ground, the first return will be the only echo and represents the bare earth surface.

The average first-return density of the NOAA Hurricane Irma topobathymetric LiDAR project was 11.42 points/m^2 (Table 12). The statistical distributions of all first return densities per 100 m x 100 m cell are portrayed in Figure 10.

Bathymetric and Ground Classified Point Densities

The density of ground and bathymetric bottom classified returns were also analyzed for this project. Terrain character, land cover, and ground surface reflectivity all influenced the density of ground surface returns. In vegetated areas, fewer pulses may have penetrated the canopy, resulting in lower ground density. Similarly, the density of bathymetric bottom returns was influenced by turbidity, depth, and bottom surface reflectivity. In turbid areas, fewer pulses may have penetrated the water surface, resulting in lower bathymetric density.

The ground and bathymetric bottom classified density of LiDAR data for the NOAA Hurricane Irma project was 5.08 points/m^2 (Table 12). The statistical distributions ground classified and bathymetric bottom return densities per 100 m x 100 m cell are portrayed in Figure 11.

Table 12: Average LiDAR point densities

Density Type	Point Density
First Returns	11.42 points/m²
Ground and Bathymetric Bottom Classified Returns	5.08 points/m²
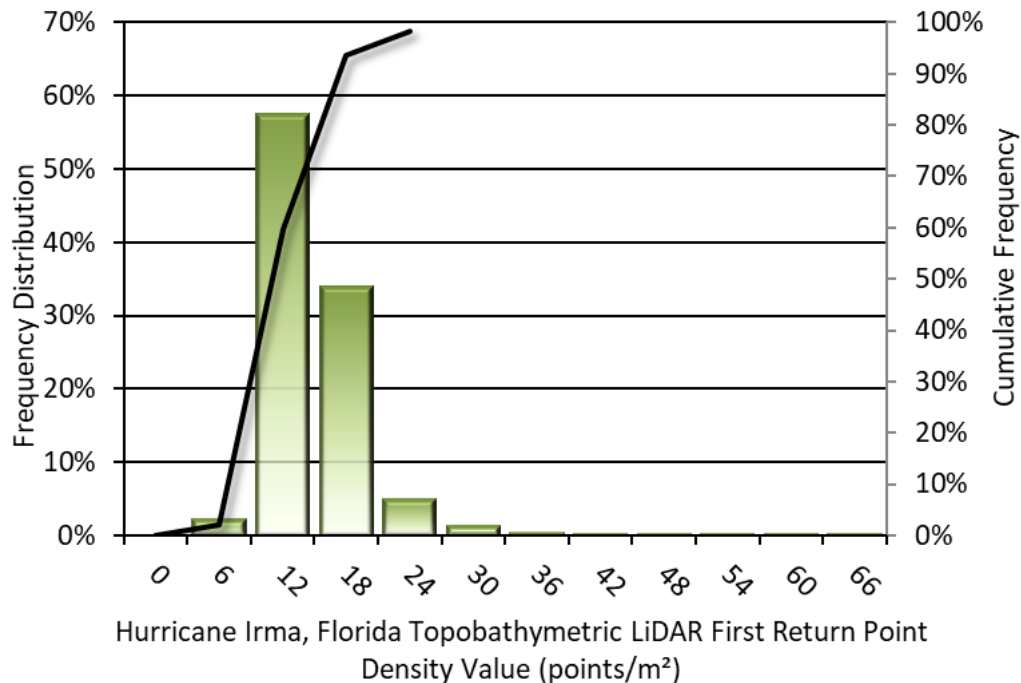
Figure 10: Frequency distribution of first return densities per 100 x 100 m cell
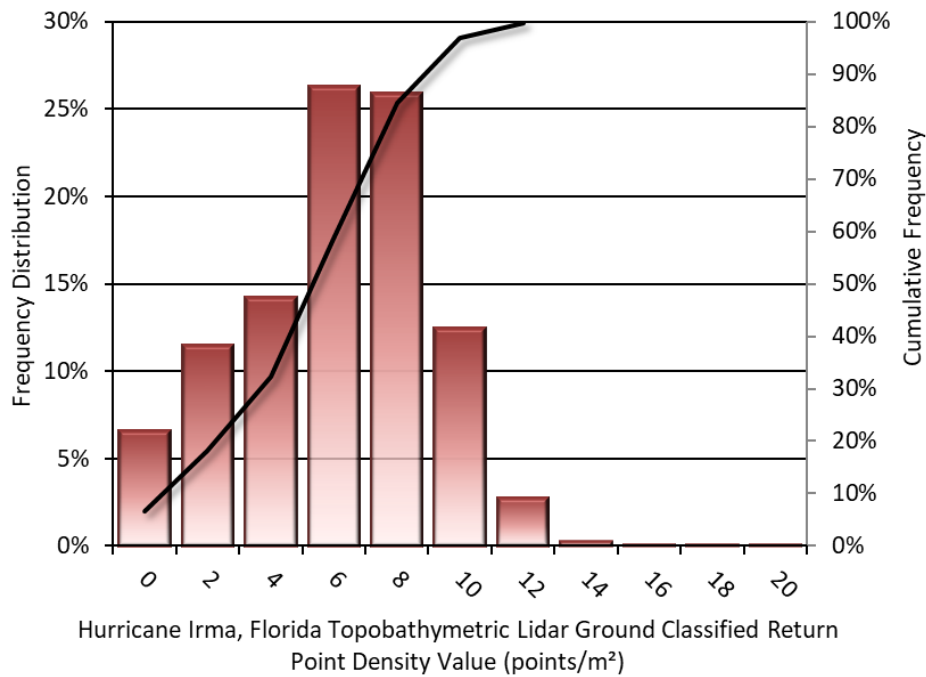
Figure 11: Frequency distribution of ground and bathymetric bottom classified return densities per 100 x 100 m cell

LiDAR Accuracy Assessments

The accuracy of the LiDAR data collection can be described in terms of absolute accuracy (the consistency of the data with external data sources) and relative accuracy (the consistency of the dataset with itself). See Appendix A for further information on sources of error and operational measures used to improve relative accuracy.

LiDAR Non-Vegetated Vertical Accuracy

Absolute accuracy was assessed using Non-vegetated Vertical Accuracy (NVA) reporting designed to meet guidelines presented in the FGDC National Standard for Spatial Data Accuracy[5]. NVA compares known ground check point data that were withheld from the calibration and post-processing of the LiDAR point cloud to the triangulated surface generated by the unclassified LiDAR point cloud as well as the derived gridded bare earth DEM. NVA compares known ground quality assurance point data collected on open, bare earth surfaces with level slope (<20°) to the triangulated surface generated by the LiDAR points. NVA is a measure of the accuracy of LiDAR point data in open areas where the LiDAR system has a high probability of measuring the ground surface and is evaluated at the 95% confidence interval (1.96 * RMSE), as shown in Table 13.

---

[5] Federal Geographic Data Committee, ASPRS POSITIONAL ACCURACY STANDARDS FOR DIGITAL GEOSPATIAL DATA EDITION 1, Version 1.0, NOVEMBER 2014. http://www.asprs.org/PAD-Division/ASPRS-POSITIONAL-ACCURACY-STANDARDS-FOR-DIGITAL-GEOSPATIAL-DATA.html.

The mean and standard deviation (sigma σ) of divergence of the ground surface model from ground check point coordinates are also considered during accuracy assessment. These statistics assume the error for x, y and z is normally distributed, and therefore the skew and kurtosis of distributions are also considered when evaluating error statistics. For the NOAA Hurricane Irma LiDAR survey, 36 ground check points were withheld from the calibration and post-processing of the LiDAR point cloud, with resulting non-vegetated vertical accuracy of 0.080 meters as compared to the unclassified LAS, and 0.083 meters as compared to the bare earth DEM, with 95% confidence.

Bathymetric (submerged) check points were also collected in order to assess the submerged surface vertical accuracy. Assessment of 509 bathymetric check points resulted in an average vertical accuracy of 0.110 meters (Table 13, Figure 14).

QSI also assessed absolute accuracy using 2,088 ground control points. Although these points were used in the calibration and post-processing of the LiDAR point cloud, they still provide a good indication of the overall accuracy of the LiDAR dataset, and therefore have been provided in Table 13 and Figure 15.

Table 13: Absolute accuracy (NVA) results

	Non-Vegetated Vertical Accuracy			
	NVA - Ground Check Points (LAS)	NVA - Ground Check Points (DEM)	Bathymetric Check Points	Ground Control Points
Sample	36 points	36 points	509 points	2,088 points
95% Confidence (1.96*RMSE)	0.080 m	0.083 m	0.110 m	0.054 m
Average	0.002 m	0.002 m	0.018 m	0.004 m
Median	0.009 m	0.004 m	0.016 m	0.006 m
RMSE	0.041 m	0.043 m	0.056 m	0.027 m
Standard Deviation (1σ)	0.041 m	0.043 m	0.053 m	0.027 m
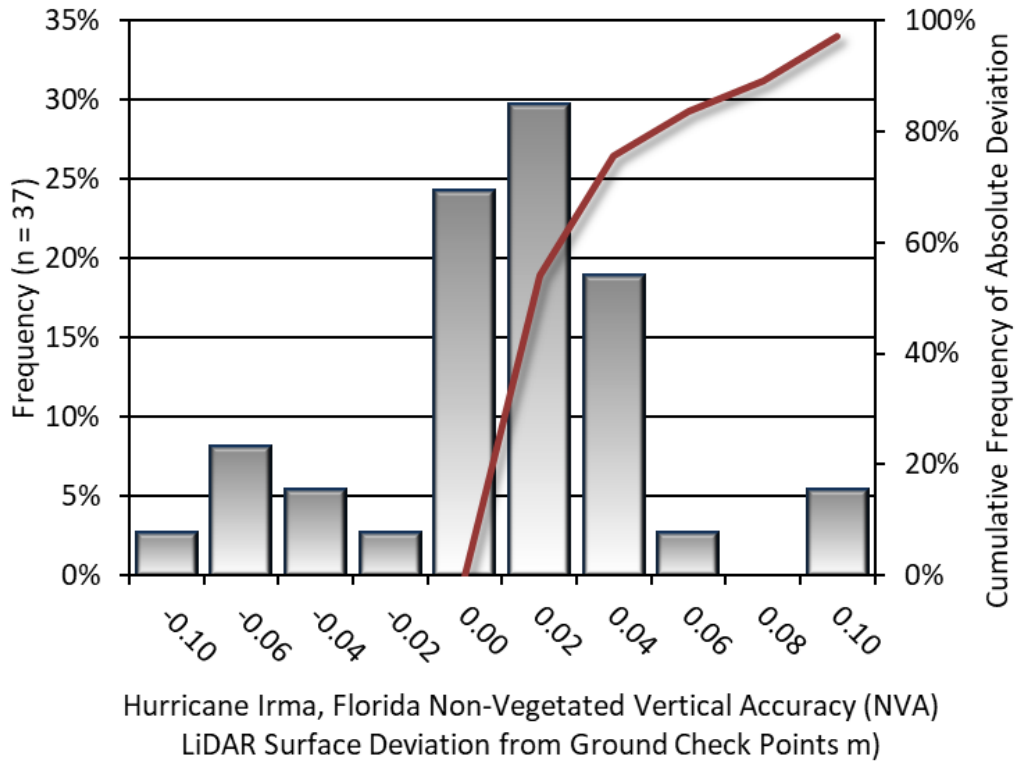
Figure 12: Frequency histogram for LiDAR surface deviation from ground check point values
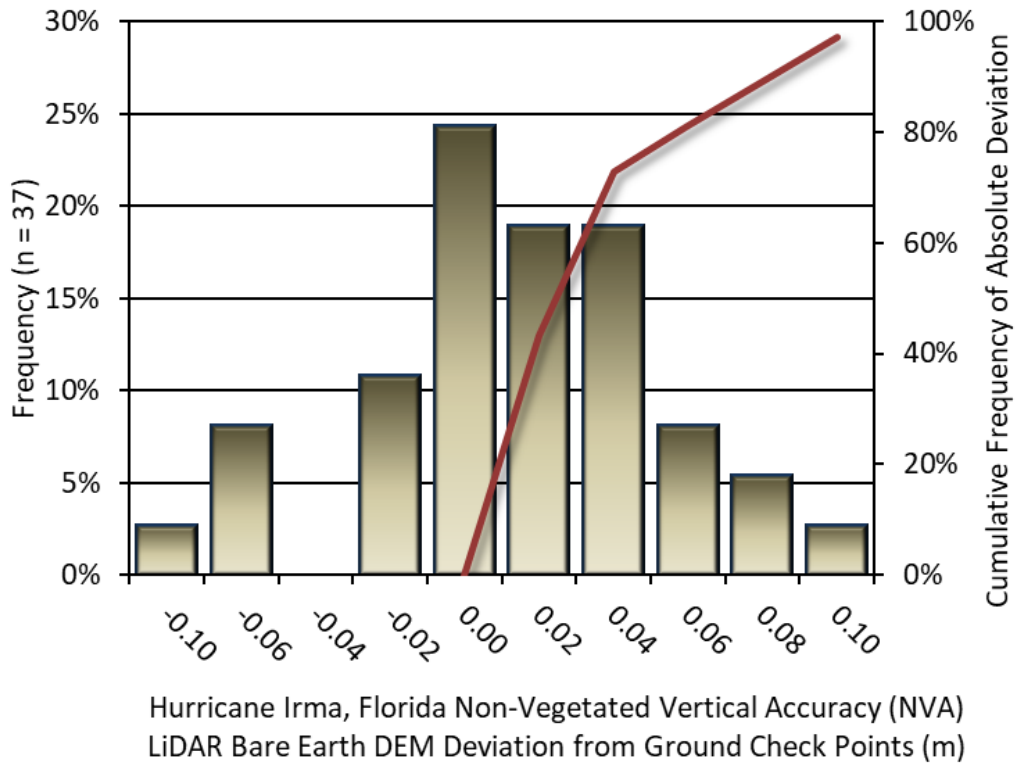
Figure 13: Frequency for LiDAR surface deviation from ground check point values against DEM surface
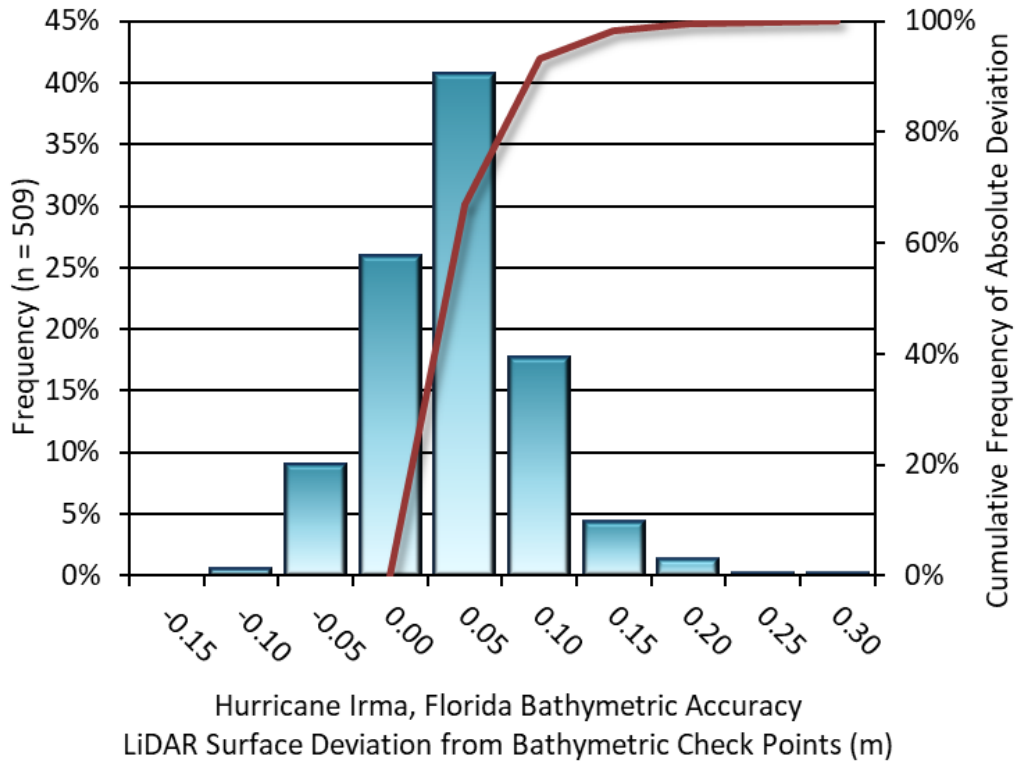
Figure 14: Frequency histogram for LiDAR surface deviation from bathymetric check point values
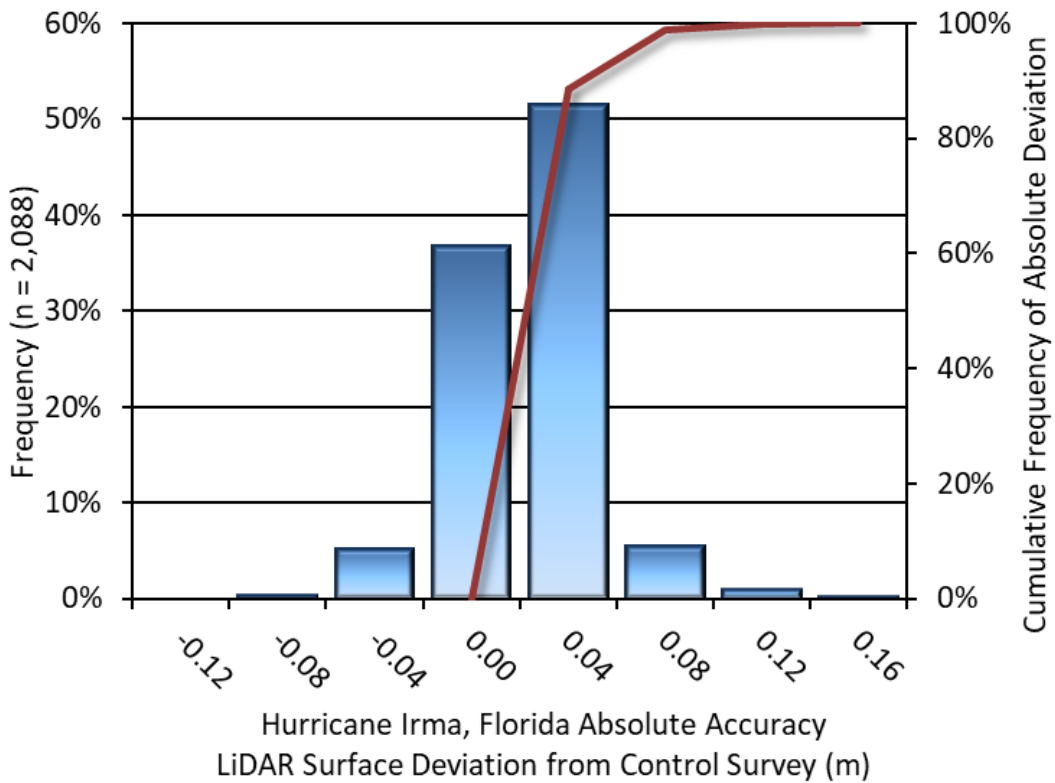
Figure 15: Frequency histogram for LiDAR surface deviation ground control point values

LiDAR Vegetated Vertical Accuracies

QSI also assessed vertical accuracy using Vegetated Vertical Accuracy (VVA) reporting. VVA compares known ground check point data collected over vegetated surfaces using land class descriptions to the triangulated ground surface generated by the ground classified LiDAR points. VVA is evaluated at the 95th percentile (Table 14, Figure 16).

Table 14: Vegetated Vertical Accuracy for the NOAA Hurricane Irma Project

Vegetated Vertical Accuracy (VVA)	
Sample	22 points
Average Dz	0.061 m
Median	0.047 m
RMSE	0.084 m
Standard Deviation (1σ)	0.060 m
95th Percentile	0.129 m
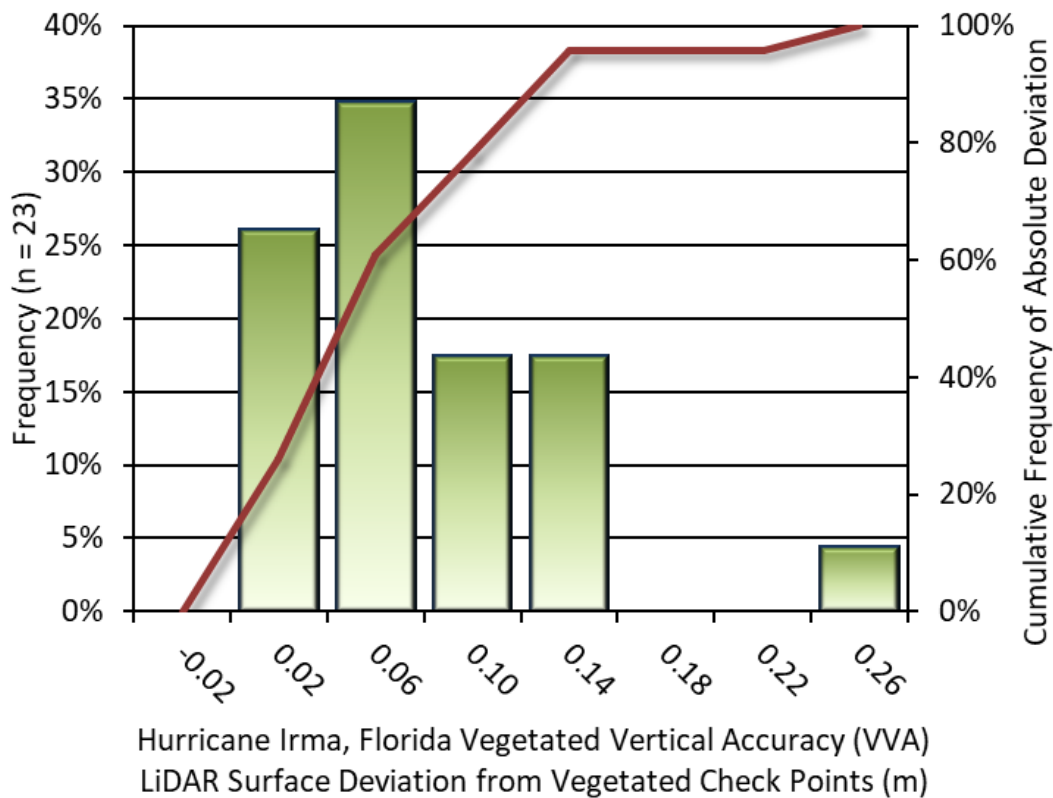
Figure 16: Frequency histogram for LiDAR surface deviation from all land cover class point values (VVA)

LiDAR Relative Vertical Accuracy

Relative vertical accuracy refers to the internal consistency of the data set as a whole: the ability to place an object in the same location given multiple flight lines, GPS conditions, and aircraft attitudes. When the LiDAR system is well calibrated, the swath-to-swath vertical divergence is low (<0.10 meters). The relative vertical accuracy was computed by comparing the ground surface model of each individual flight line with its neighbors in overlapping regions. The average (mean) line to line relative vertical accuracy for the NOAA Hurricane Irma LiDAR project was 0.035 meters (Table 15, Figure 17).

Table 15: Relative accuracy results

Relative Accuracy	
Sample	1,470 surfaces
Average	0.035 m
Median	0.035 m
RMSE	0.047 m
Standard Deviation (1σ)	0.020 m
1.96σ	0.039 m

Hurricane Irma, Florida Topobathymetric Lidar Relative Vertical Accuracy (m)
Total Compared Points (n = 18,299,370,949)
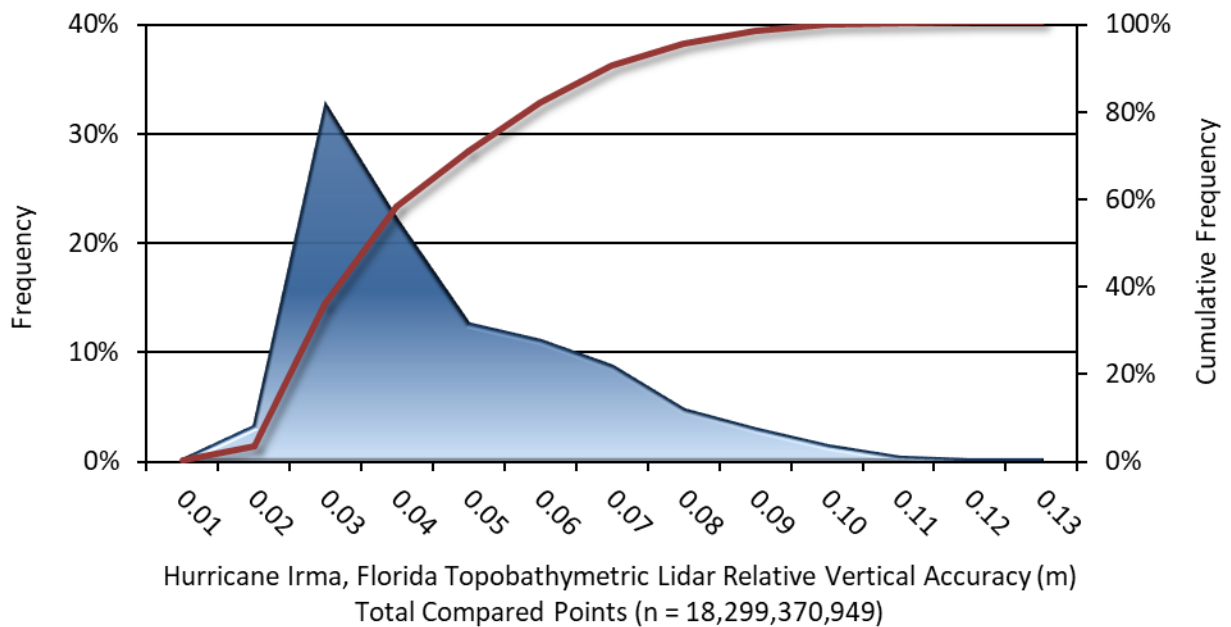
Figure 17: Frequency plot for relative vertical accuracy between flight lines

LiDAR Horizontal Accuracy

LiDAR horizontal accuracy is a function of Global Navigation Satellite System (GNSS) derived positional error, flying altitude, and INS derived attitude error. The obtained $RMSE_r$ value is multiplied by a conversion factor of 1.7308 to yield the horizontal component of the National Standards for Spatial Data Accuracy (NSSDA) reporting standard where a theoretical point will fall within the obtained radius 95 percent of the time. Based on a flying altitude of 400 meters, an IMU error of 0.005 decimal degrees, and a GNSS positional error of 0.023 meters, this project was compiled to meet 0.115 m horizontal accuracy at the 95% confidence level.

Table 16: Horizontal Accuracy

Horizontal Accuracy	
$RMSE_r$	0.067 m
ACC_r	0.115 m

Digital Imagery Accuracy Assessment

Image accuracy was measured by air target locations and independent ground survey points. QSI provided imagery accuracy assessment along with the imagery deliverable reporting (Table 2), as **_FL_1806_NOAA_Florida_Keys_Topobathy_AT_Report.doc._**

Lessons Learned

The NOAA Supplemental Hurricane Irma, Florida Keys project was the largest topobathymetric data acquisition and processing project ever undertaken by Quantum Spatial and required an immense amount of ground and airborne survey coordination by QSI's acquisition team. Acquisition efforts were successful overall but lidar processing presented a challenge due to the immense volume of data collected. Digital Imagery encountered seasonal weather challenges as well, which ultimately required a significant amount of the digital imagery to be re-flown.

The biggest challenges encountered during data processing, aside from data volume, involved environmental conditions including a large amount of aquatic vegetation, classification of reef structures, and a large amount of boats present in the project area. Boats presented a significant challenge in water surface modeling efforts required to apply an accurate refraction correction.

TPU was closely coordinated with help from NOAA developers and will require refinement and feedback from NOAA to determine the most appropriate deliverable format for future topobathymetric lidar and shoreline mapping projects.

1-sigma (σ) Absolute Deviation: Value for which the data are within one standard deviation (approximately 68th percentile) of a normally distributed data set.

1.96 * RMSE Absolute Deviation: Value for which the data are within two standard deviations (approximately 95th percentile) of a normally distributed data set, based on the FGDC standards for Non-vegetated Vertical Accuracy (FVA) reporting.

Accuracy: The statistical comparison between known (surveyed) points and laser points. Typically measured as the standard deviation (sigma σ) and root mean square error (RMSE).

> **Absolute Accuracy:** The vertical accuracy of LiDAR data is described as the mean and standard deviation (sigma σ) of divergence of LiDAR point coordinates from ground survey point coordinates. To provide a sense of the model predictive power of the dataset, the root mean square error (RMSE) for vertical accuracy is also provided. These statistics assume the error distributions for x, y and z are normally distributed, and thus we also consider the skew and kurtosis of distributions when evaluating error statistics.

> **Relative Accuracy:** Relative accuracy refers to the internal consistency of the data set; i.e., the ability to place a laser point in the same location over multiple flight lines, GPS conditions and aircraft attitudes. Affected by system attitude offsets, scale and GPS/IMU drift, internal consistency is measured as the divergence between points from different flight lines within an overlapping area. Divergence is most apparent when flight lines are opposing. When the LiDAR system is well calibrated, the line-to-line divergence is low (<10 cm).

> **Root Mean Square Error (RMSE):** A statistic used to approximate the difference between real-world points and the LiDAR points. It is calculated by squaring all the values, then taking the average of the squares and taking the square root of the average.

Data Density: A common measure of LiDAR resolution, measured as points per square meter.

Digital Elevation Model (DEM): File or database made from surveyed points, containing elevation points over a contiguous area. Digital terrain models (DTM) and digital surface models (DSM) are types of DEMs. DTMs consist solely of the bare earth surface (ground points), while DSMs include information about all surfaces, including vegetation and man-made structures.

Intensity Values: The peak power ratio of the laser return to the emitted laser, calculated as a function of surface reflectivity.

Nadir: A single point or locus of points on the surface of the earth directly below a sensor as it progresses along its flight line.

Overlap: The area shared between flight lines, typically measured in percent. 100% overlap is essential to ensure complete coverage and reduce laser shadows.

Pulse Rate (PR): The rate at which laser pulses are emitted from the sensor; typically measured in thousands of pulses per second (kHz).

Pulse Returns: For every laser pulse emitted, the number of wave forms (i.e., echoes) reflected back to the sensor. Portions of the wave form that return first are the highest element in multi-tiered surfaces such as vegetation. Portions of the wave form that return last are the lowest element in multi-tiered surfaces.

Real-Time Kinematic (RTK) Survey: A type of surveying conducted with a GPS base station deployed over a known monument with a radio connection to a GPS rover. Both the base station and rover receive differential GPS data and the baseline correction is solved between the two. This type of ground survey is accurate to 1.5 cm or less.

Post-Processed Kinematic (PPK) Survey: GPS surveying is conducted with a GPS rover collecting concurrently with a GPS base station set up over a known monument. Differential corrections and precisions for the GNSS baselines are computed and applied after the fact during processing. This type of ground survey is accurate to 1.5 cm or less.

Scan Angle: The angle from nadir to the edge of the scan, measured in degrees. Laser point accuracy typically decreases as scan angles increase.

Native LiDAR Density: The number of pulses emitted by the LiDAR system, commonly expressed as pulses per square meter.

Relative Accuracy Calibration Methodology:

Manual System Calibration: Calibration procedures for each mission require solving geometric relationships that relate measured swath-to-swath deviations to misalignments of system attitude parameters. Corrected scale, pitch, roll and heading offsets were calculated and applied to resolve misalignments. The raw divergence between lines was computed after the manual calibration was completed and reported for each survey area.

Automated Attitude Calibration: All data were tested and calibrated using TerraMatch automated sampling routines. Ground points were classified for each individual flight line and used for line-to-line testing. System misalignment offsets (pitch, roll and heading) and scale were solved for each individual mission and applied to respective mission datasets. The data from each mission were then blended when imported together to form the entire area of interest.

Automated Z Calibration: Ground points per line were used to calculate the vertical divergence between lines caused by vertical GPS drift. Automated Z calibration was the final step employed for relative accuracy calibration.

LiDAR accuracy error sources and solutions:

Type of Error	Source	Post Processing Solution
GPS (Static/Kinematic)	Long Base Lines	None
	Poor Satellite Constellation	None
	Poor Antenna Visibility	Reduce Visibility Mask
Relative Accuracy	Poor System Calibration	Recalibrate IMU and sensor offsets/settings
	Inaccurate System	None
Laser Noise	Poor Laser Timing	None
	Poor Laser Reception	None
	Poor Laser Power	None
	Irregular Laser Shape	None

Operational measures taken to improve relative accuracy:

Low Flight Altitude: Terrain following was employed to maintain a constant above ground level (AGL). Laser horizontal errors are a function of flight altitude above ground (about 1/3000th AGL flight altitude).

Focus Laser Power at narrow beam footprint: A laser return must be received by the system above a power threshold to accurately record a measurement. The strength of the laser return (i.e., intensity) is a function of laser emission power, laser footprint, flight altitude and the reflectivity of the target. While surface reflectivity cannot be controlled, laser power can be increased and low flight altitudes can be maintained.

Reduced Scan Angle: Edge-of-scan data can become inaccurate. The scan angle was reduced to a maximum of ±20° from nadir, creating a narrow swath width and greatly reducing laser shadows from trees and buildings.

Quality GPS: Flights took place during optimal GPS conditions (e.g., 6 or more satellites and PDOP [Position Dilution of Precision] less than 3.0). Before each flight, the PDOP was determined for the survey day. During all flight times, a dual frequency DGPS base station recording at 1 second epochs was utilized and a maximum baseline length between the aircraft and the control points was less than 13 nm at all times.

Ground Survey: Ground survey point accuracy (<1.5 cm RMSE) occurs during optimal PDOP ranges and targets a minimal baseline distance of 4 miles between GPS rover and base. Robust statistics are, in part, a function of sample size (n) and distribution. Ground survey points are distributed to the extent possible throughout multiple flight lines and across the survey area.

50% Side-Lap (100% Overlap): Overlapping areas are optimized for relative accuracy testing. Laser shadowing is minimized to help increase target acquisition from multiple scan angles. Ideally, with a 50% side-lap, the nadir portion of one flight line coincides with the swath edge portion of overlapping flight lines. A minimum of 50% side-lap with terrain-followed acquisition prevents data gaps.

Opposing Flight Lines: All overlapping flight lines have opposing directions. Pitch, roll and heading errors are amplified by a factor of two relative to the adjacent flight line(s), making misalignments easier to detect and resolve.

July 31, 2019
Revised: August 26, 2019

Florida Keys Topobathymetric LiDAR

Ground Survey Report

National Oceanic and Atmospheric Administration
U.S. Department of Commerce

National Oceanic and Atmospheric Administration (NOAA)
Gregory Stinner
Attn: N/NGS3; SSMC-3 Sta. 8245
1315 East West Highway
Silver Spring, MD 20910

quantum SPATIAL

QSI Corvallis
1100 NE Circle Blvd, Ste. 126
Corvallis, OR 97330
PH: 541-752-1204

TABLE OF CONTENTS

Cover Photo: Seaside view in the NOAA Hurricane Irma project. Credit: QSI Ground Professional Camden Beeghly.

QSI ground survey vehicle on Fat Deer Key.

Credit: QSI Ground Professional Camden Beeghly

In August 2018, Quantum Spatial (QSI) was contracted by the National Oceanic and Atmospheric Administration (NOAA), to collect topographic Light Detection and Ranging (LiDAR) data and digital imagery from November of 2018 through March of 2019, for the NOAA Hurricane Irma site along the coast of the Florida panhandle. In total, the Florida Keys project site extends approximately 176 miles along the Florida coast, beginning near Miami and stretching west through Marquesas Keys. Data were collected to aid NOAA in modeling the topographic and geophysical properties of the study area to support accurate measurement and mapping of the national shoreline, and marine resource management.

This report accompanies the collected topobathymetric LiDAR data and digital imagery and documents the ground survey efforts conducted to support the airborne acquisition.

Vicinity of aerial target AT026 on Ramrod Key.

Credit: QSI Ground Professional Emily Gottesfeld

Ground control surveys including monumentation and aerial target collection were conducted to support the airborne acquisition. Ground control data were used to geospatially correct the aircraft positional coordinate data and to perform adjustments on orthoimagery products.

Static Control

Permanent continuously operating base stations from the Trimble VRS-Now[6] and the Florida Permanent Reference Network (FPRN[7]) were utilized for the ground survey, including aerial targets, LiDAR vertical control, and LiDAR vertical check points. Real-Time Network (RTN) base stations were selected with consideration for satellite visibility, RTN connectivity, and optimal location for survey point and mission planning.

No new monuments were set for this ground survey.

Base Stations

QSI utilized nine permanent RTN stations for the NOAA Hurricane Irma project. Three base stations were from the VRS-Now network and six were from the FPRN. The position, precision, and network of each base station have been provided in Table 17. Record positions were held for all base stations.

---

[6] https://positioningservices.trimble.com/services/vrs/vrs-now/

[7] https://www.fdot.gov/geospatial/fprn.shtm

QSI triangulated static Global Navigation Satellite System (GNSS) data (1 Hz recording frequency) from each base station with nearby Continuously Operating Reference Stations (CORS) using the Online Positioning User Service (OPUS[8]) to ensure alignment with the National Spatial Reference System (NSRS), updating record positions as necessary. Multiple independent sessions over the same monument were processed to confirm antenna height measurements and to refine position accuracy. The five NGS CORS utilized during OPUS Project processing are listed in Table 18.

Table 17: Permanent Real-Time Network (RTN) stations utilized for the NOAA Hurricane Irma acquisition. Coordinates are on the NAD83 (2011) datum, epoch 2010.00. Precision values shown are for the 68% (1-sigma) confidence interval. Units are in meters.

Station ID	Latitude	Longitude	Ellips.	σ X	σ Y	σ Z	Network	Held?
FLKW	24° 33' 13.26664"	-81° 45' 15.39914"	-10.257	0.001	0.000	0.006	FPRN	YES
FLKW*	24° 39' 33.67173"	-81° 31' 20.54518"	-11.211	0.005	0.002	0.006	VRSNOW	YES
FLMA	24° 43' 06.59490"	-81° 04' 06.74239"	-11.711	0.004	0.001	0.013	FPRN	YES
FLMB	25° 46' 57.83786"	-80° 08' 14.16764"	-15.518	0.001	0.001	0.003	FPRN	YES
FLMK	24° 43' 33.36203"	-81° 02' 56.70329"	-13.903	0.000	0.001	0.006	FPRN	YES
FLPK	24° 57' 47.22531"	-80° 34' 05.39838"	-13.201	0.001	0.000	0.017	FPRN	YES
FLUM	25° 43' 54.86870"	-80° 09' 48.52710"	-5.285	0.005	0.002	0.006	VRSNOW	YES
HMST	25° 28' 13.58298"	-80° 29' 19.63111"	-16.134	0.001	0.001	0.023	VRSNOW	YES
HOME	25° 30' 03.79565"	-80° 33' 00.43217"	-19.134	0.002	0.005	0.013	FPRN	YES

* Trimble VRS-Now and FPRN independently include a station named FLKW. It is not a duplicate.

Table 18: NGS CORS utilized with OPUS Project. Published NAD83(2011) coordinates were held and can be retrieved from http://www.ngs.noaa.gov/CORS/.

CORS used in OPUS Project		
FLBN	FLF1	GACR
GNVL	ZMA1	

Network Accuracy

Base station coordinates were established according to the national standard for geodetic control networks, as specified in the Federal Geographic Data Committee (FGDC) Geospatial Positioning Accuracy Standards for geodetic networks.[9] This standard provides guidelines for classification of monument quality at the 95% confidence interval as a basis for comparing the quality of one control network to another. The monument rating for this project is shown in Table 19.

---

[8] OPUS is a free service provided by the National Geodetic Survey to process corrected monument positions. http://www.ngs.noaa.gov/OPUS.

[9] Federal Geographic Data Committee, Geospatial Positioning Accuracy Standards (FGDC-STD-007.2-1998). Part 2: Standards for Geodetic Networks, Table 2.1, page 2-3. http://www.fgdc.gov/standards/projects/FGDC-standards-projects/accuracy/part2/chapter2

Table 19: Federal Geographic Data Committee monument rating for network accuracy

Direction	Rating
1.96 * St Dev $_{NE}$:	0.020 m
1.96 * St Dev $_{Z}$:	0.050 m

Aerial Target Collection

Aerial targets were located throughout the project area in order to geospatially correct the orthoimagery. Each target was precisely located using one or more points, depending on the methodology used, each point being at least three times as accurate as the orthophotographs in accordance with ASPRS Positional Accuracy Standards for Digital Geospatial Data (2014).

Permanent and existing photo-identifiable features such as stop bars and turn lane arrows were favored to ensure that the feature would not be prone to disturbance between the time of the ground survey and aerial acquisition.

The Real-Time Kinematic (RTK) survey technique was utilized for the geolocation of aerial targets. For this method a cellular connection provided kinematic corrections from a regional Real-Time Network (RTN) to a nearby roving GNSS receiver. QSI equipment used for the ground survey is summarized in Table 7.

Table 20: QSI equipment identification table. Does not include CORS antennas.

Receiver Model	Antenna	OPUS Antenna ID	Serial Numbers	Use
Trimble R8 Model 2	Integrated Antenna	TRMR8_GNSS	0649, 8595	Rover
Trimble R8 Model 3	Integrated Antenna	TRMR8_GNSS3	9860	Rover

When collecting RTK data, the rover records data while stationary for five seconds, then calculates the pseudorange position using at least three one-second epochs. Relative errors for any position must be less than 1.5 cm horizontal and 2.0 cm vertical in order to be accepted. All measurements were made during periods with a Position Dilution of Precision (PDOP) of ≤ 3.0 with at least six satellites in view of the stationary and roving receivers. RTK post-processing was conducted using Trimble Business Center version 4.

All ground surveys were tied to the NAD83(2011) reference frame via the NGS CORS network and achieved the accuracy required for this project. A total of 93 aerial targets were collected using 278 occupations for the NOAA Hurricane Irma project. Of these, 79 targets were utilized as control during orthophoto processing, while 14 were withheld from processing for final quality checks.

Target Types

Aerial targets for orthophoto processing were collected a myriad of existing photo-identifiable objects in order to geospatially correct the orthoimagery. These objects were selected based on their stability, likelihood of obstruction, and spectral contrast against surrounding objects. Table 21 contains a representative photograph of each aerial target encountered for this project.

These photographs are meant to convey the general meaning of a target type and do not imply that all targets of a particular type look exactly identical, nor do they imply that the same reference points were recorded for every target of a particular type.

Target Positions

Aerial target positions for the NOAA Hurricane Irma project are summarized below in Table 22. A copy of NOAA Form 76-53 – Control Station Identification has been filled out for every aerial target and may be found in the "NOAA FK Form 76-53.zip" archive that accompanies this report. This form contains more detailed information regarding each aerial target.

Targets recorded from multiple reference points are reported as having multiple occupations. In such a case the reported position is approximate and is not necessarily the position held during orthophoto rectification. Multiple reference points were recorded during the ground survey to ensure that each target could be identified and referenced in the orthoimagery even if the target was partially obscured at the time of acquisition.

Session lengths are shown in Table 22 in minutes and seconds. The survey methods shown were described in detail earlier in this report. The horizontal and vertical precision of each target is shown, in meters, based on the 68% confidence interval, or the root mean square error (RMSE) of the position. Points named AT000 were used as control during orthophoto processing; points named QA000 were withheld from production and used as a final quality check on the photos.

Table 21: Representative photographs of each aerial target type utilized in the NOAA Hurricane Irma project

Type	Representative Photograph	Type	Representative Photograph
Arrow		Basketball Court	
Chevron		Concrete Corner	
Cross		Crosswalk	
Diamond		Parking Lines	
Stop Bar		Traffic Lines	

Table 22: List of all aerial targets. Horizontal coordinates are in the UTM17 coordinate system and referenced to the NAD83(2011) datum. Ellipsoid heights are referenced to the GRS80 ellipsoid.

PID	Easting (m)	Northing (m)	Ellipsoid Height (m)	Occ. Count	Avg. Session Length	Ref. Base	Horiz. RMSE (m)	Vert. RMSE (m)	Target Type
AT001A	417949.966	2714961.846	-19.560	1	0:00:09	FLKW*	0.011	0.019	Arrow
AT001B	417949.002	2714962.519	-19.582	1	0:00:05	FLKW*	0.011	0.018	Arrow
AT001C	417968.140	2714930.855	-19.731	1	0:00:24	FLKW*	0.011	0.020	Arrow
AT001D	417969.087	2714930.160	-19.747	1	0:00:05	FLKW*	0.011	0.019	Arrow
AT002A	418223.146	2716476.764	-21.056	1	0:00:05	FLKW*	0.010	0.017	Concrete Corner
AT002B	418219.031	2716474.757	-21.000	1	0:00:05	FLKW*	0.011	0.018	Concrete Corner
AT003A	421766.214	2717008.298	-20.023	1	0:00:05	FLKW*	0.011	0.019	Stop Bar
AT003B	421771.277	2717014.887	-20.039	1	0:00:06	FLKW*	0.011	0.020	Stop Bar
AT004A	421366.159	2715389.656	-20.891	1	0:00:05	FLKW*	0.009	0.018	Traffic Lines
AT004B	421362.149	2715389.024	-20.945	1	0:00:05	FLKW*	0.009	0.018	Traffic Lines
AT005A	420163.142	2716096.438	-20.678	1	0:00:05	FLKW*	0.009	0.015	Basketball Court
AT005B	420154.937	2716109.259	-20.565	1	0:00:05	FLKW*	0.011	0.018	Basketball Court
AT005C	420133.656	2716094.951	-20.527	1	0:00:05	FLKW*	0.011	0.017	Basketball Court
AT005D	420141.814	2716082.043	-20.568	1	0:00:05	FLKW*	0.010	0.017	Basketball Court
AT006A	423734.984	2715602.709	-20.873	1	0:00:05	FLKW*	0.007	0.015	Stop Bar
AT006B	423729.785	2715601.658	-20.867	1	0:00:05	FLKW*	0.007	0.015	Stop Bar
AT007A	423684.620	2717698.444	-20.870	1	0:00:09	FLKW*	0.010	0.017	Concrete Corner
AT007B	423691.676	2717693.718	-20.871	1	0:00:05	FLKW*	0.011	0.019	Concrete Corner
AT007C	423688.329	2717696.638	-20.830	1	0:00:06	FLKW*	0.010	0.018	Arrow
AT007D	423689.352	2717696.566	-20.839	1	0:00:05	FLKW*	0.010	0.018	Arrow
AT010A	433672.198	2718557.366	-21.204	1	0:00:05	FLKW*	0.008	0.014	Stop Bar
AT010B	433668.736	2718556.933	-21.193	1	0:00:05	FLKW*	0.007	0.013	Stop Bar
AT011A	431839.236	2717070.848	-20.308	1	0:00:05	FLKW*	0.006	0.013	Chevron
AT011B	431840.239	2717071.883	-20.298	1	0:00:05	FLKW*	0.007	0.014	Chevron
AT013A	433994.139	2720722.999	-19.660	1	0:00:05	FLKW*	0.012	0.018	Arrow
AT013B	433996.564	2720721.964	-19.704	1	0:00:05	FLKW*	0.009	0.014	Arrow
AT014A	437325.812	2722427.341	-18.953	1	0:00:05	FLKW*	0.009	0.016	Concrete Corner
AT014B	437327.159	2722424.504	-18.463	1	0:00:05	FLKW*	0.009	0.016	Concrete Corner
AT015A	440035.643	2724029.125	-19.669	1	0:00:05	FLKW*	0.006	0.010	Crosswalk
AT015B	440037.458	2724025.992	-19.758	1	0:00:05	FLKW*	0.006	0.010	Crosswalk
AT016A	442813.820	2725898.435	-20.155	1	0:00:05	FLKW	0.008	0.014	Arrow
AT016B	442813.467	2725897.205	-20.123	1	0:00:05	FLKW	0.008	0.013	Arrow
AT016C	442815.198	2725898.168	-20.128	1	0:00:05	FLKW	0.008	0.013	Arrow
AT017A	445482.615	2728682.886	-20.962	1	0:00:05	FLKW*	0.007	0.013	Chevron
AT017B	445483.800	2728681.897	-20.973	1	0:00:05	FLKW*	0.007	0.013	Chevron
AT018A	446413.207	2727289.460	-20.345	1	0:00:05	FLKW*	0.006	0.010	Concrete Corner
AT018B	446417.634	2727296.430	-20.027	1	0:00:05	FLKW*	0.006	0.010	Concrete Corner
AT019A	449456.894	2728134.454	-21.003	1	0:00:06	FLKW*	0.005	0.008	Stop Bar

PID	Easting (m)	Northing (m)	Ellipsoid Height (m)	Occ. Count	Avg. Session Length	Ref. Base	Horiz. RMSE (m)	Vert. RMSE (m)	Target Type
AT019B	449457.232	2728137.824	-21.040	1	0:00:05	FLKW*	0.005	0.009	Stop Bar
AT020A	451401.199	2725891.332	-21.164	1	0:00:05	FLKW*	0.007	0.011	Stop Bar
AT020B	451397.389	2725890.101	-21.133	1	0:00:05	FLKW*	0.006	0.011	Stop Bar
AT021	449463.084	2731186.007	-21.143	1	0:03:00	FLKW	0.006	0.011	Cross
AT022A	449453.889	2731258.571	-20.994	1	0:00:05	FLKW	0.010	0.018	Concrete Corner
AT022B	449462.914	2731257.521	-20.982	1	0:00:05	FLKW	0.009	0.019	Concrete Corner
AT023A	453200.941	2727638.016	-19.160	1	0:00:05	FLKW*	0.008	0.013	Concrete Corner
AT023B	453187.916	2727642.025	-18.973	1	0:00:05	FLKW*	0.008	0.013	Concrete Corner
AT024	455058.642	2730069.558	-21.069	1	0:00:05	FLKW*	0.006	0.010	Concrete Corner
AT025A	458992.958	2726238.685	-21.162	1	0:00:05	FLKW	0.009	0.015	Stop Bar
AT025B	458997.254	2726238.639	-21.198	1	0:00:05	FLKW	0.010	0.017	Stop Bar
AT025C	458997.245	2726238.059	-21.216	1	0:00:05	FLKW	0.009	0.016	Stop Bar
AT026A	457982.536	2727886.304	-21.453	1	0:00:05	FLKW	0.009	0.015	Stop Bar
AT026B	457983.090	2727886.270	-21.500	1	0:00:05	FLKW	0.010	0.016	Stop Bar
AT026C	457982.495	2727889.442	-21.462	1	0:00:05	FLKW	0.010	0.016	Stop Bar
AT026D	457983.053	2727889.465	-21.514	1	0:00:05	FLKW	0.011	0.017	Stop Bar
AT027A	454373.907	2734273.567	-20.861	1	0:00:06	FLKW	0.009	0.019	Arrow
AT027B	454373.894	2734273.332	-20.861	1	00:05.8	FLKW	0.009	0.018	Arrow
AT028A	459976.864	2730403.043	-21.117	1	0:00:27	FLMK	0.013	0.020	Stop Bar
AT028B	459976.294	2730403.066	-21.141	1	0:00:08	FLMK	0.013	0.020	Stop Bar
AT028C	459976.656	2730398.863	-21.118	1	0:00:20	FLMK	0.013	0.020	Stop Bar
AT028D	459976.148	2730398.865	-21.120	1	0:00:25	FLMK	0.013	0.020	Stop Bar
AT029A	457002.802	2730834.582	-20.990	1	0:00:22	FLMK	0.013	0.020	Concrete Corner
AT029B	457002.265	2730835.247	-20.986	1	0:00:06	FLMK	0.012	0.019	Concrete Corner
AT029C	457001.081	2730834.344	-21.100	1	0:00:05	FLMK	0.012	0.019	Concrete Corner
AT029D	457001.610	2730833.663	-21.078	1	0:00:06	FLMK	0.012	0.018	Concrete Corner
AT030A	461048.992	2726831.252	-21.063	1	00:24.2	FLKW	0.013	0.020	Stop Bar
AT030B	461048.405	2726831.186	-21.095	1	0:00:09	FLKW	0.013	0.019	Stop Bar
AT030C	461048.737	2726835.033	-21.065	1	00:18.2	FLKW	0.013	0.020	Stop Bar
AT030D	461048.151	2726835.029	-21.112	1	0:00:09	FLKW	0.013	0.018	Stop Bar
AT031A	460748.677	2728066.795	-19.615	1	0:00:17	FLMK	0.009	0.020	Stop Bar
AT031B	460748.682	2728069.184	-19.791	1	0:00:08	FLMK	0.009	0.019	Stop Bar
AT032A	459521.589	2734421.354	-20.988	1	0:00:13	FLKW	0.010	0.020	Stop Bar
AT032B	459521.576	2734421.944	-20.987	1	00:12.8	FLKW	0.010	0.020	Stop Bar
AT032C	459524.856	2734421.321	-20.921	1	00:09.8	FLKW	0.010	0.020	Stop Bar
AT033A	466506.823	2731862.931	-21.219	1	0:00:05	FLMK	0.011	0.019	Stop Bar
AT033B	466507.125	2731862.937	-21.207	1	0:00:05	FLMK	0.011	0.019	Stop Bar
AT033C	466506.660	2731872.105	-21.218	1	0:00:05	FLMK	0.011	0.018	Stop Bar
AT033D	466506.909	2731872.117	-21.199	1	00:05.8	FLMK	0.011	0.018	Stop Bar
AT034A	463778.754	2730759.697	-21.149	1	0:00:15	FLMK	0.011	0.020	Stop Bar

PID	Easting (m)	Northing (m)	Ellipsoid Height (m)	Occ. Count	Avg. Session Length	Ref. Base	Horiz. RMSE (m)	Vert. RMSE (m)	Target Type
AT034B	463778.201	2730759.532	-21.137	1	00:05.8	FLMK	0.011	0.019	Stop Bar
AT034C	463777.245	2730764.756	-21.200	1	0:00:06	FLMK	0.011	0.020	Stop Bar
AT034D	463776.676	2730764.576	-21.202	1	00:05.2	FLMK	0.010	0.018	Stop Bar
AT035A	466410.005	2726063.149	-17.844	1	0:00:05	FLMK	0.010	0.017	Stop Bar
AT035B	466410.381	2726063.594	-17.830	1	0:00:05	FLMK	0.010	0.017	Stop Bar
AT035C	466403.552	2726065.928	-17.881	1	00:05.2	FLMK	0.010	0.017	Stop Bar
AT035D	466403.774	2726066.504	-17.878	1	0:00:05	FLMK	0.010	0.017	Stop Bar
AT036A	455189.656	2725803.394	-20.807	1	0:00:05	FLKW*	0.006	0.012	Stop Bar
AT036B	455193.998	2725807.893	-20.784	1	0:00:05	FLKW*	0.006	0.012	Stop Bar
AT036C	455193.571	2725808.333	-20.774	1	0:00:05	FLKW*	0.006	0.012	Stop Bar
AT036D	455189.201	2725803.789	-20.816	1	0:00:05	FLKW*	0.006	0.012	Stop Bar
AT037A	469333.782	2726613.934	-17.974	1	00:07.2	FLMK	0.014	0.019	Stop Bar
AT037B	469333.509	2726614.414	-17.975	1	00:05.2	FLMK	0.013	0.018	Stop Bar
AT037C	469329.508	2726611.517	-18.013	1	0:00:10	FLMK	0.014	0.020	Stop Bar
AT037D	469329.052	2726611.943	-18.044	1	00:18.2	FLMK	0.013	0.019	Stop Bar
AT038A	474322.937	2728309.837	-19.917	1	0:00:05	FLMK	0.014	0.018	Concrete Corner
AT038B	474322.797	2728310.240	-19.910	1	0:00:05	FLMK	0.012	0.017	Concrete Corner
AT038C	474323.340	2728310.019	-19.910	1	00:05.4	FLMK	0.014	0.019	Concrete Corner
AT038D	474323.151	2728310.384	-19.924	1	0:00:05	FLMK	0.014	0.019	Concrete Corner
AT039A	474970.411	2728610.074	-18.485	1	00:05.8	FLMK	0.013	0.019	Stop Bar
AT039B	474970.462	2728609.778	-18.477	1	0:00:05	FLMK	0.013	0.019	Stop Bar
AT039C	474948.551	2728606.162	-18.765	1	0:00:20	FLMK	0.013	0.020	Stop Bar
AT039D	474948.498	2728606.450	-18.761	1	0:00:08	FLMK	0.013	0.020	Stop Bar
AT040A	476796.110	2729800.145	-20.590	1	0:00:05	FLMK	0.012	0.020	Parking Lines
AT040B	476792.457	2729810.626	-21.267	1	0:00:05	FLMK	0.011	0.020	Parking Lines
AT041A	488020.909	2732557.496	-21.188	1	00:05.6	FLMK	0.008	0.013	Concrete Corner
AT041B	488021.819	2732557.654	-21.150	1	00:05.6	FLMK	0.008	0.013	Concrete Corner
AT041C	488021.941	2732556.900	-21.142	1	00:05.2	FLMK	0.008	0.013	Concrete Corner
AT041D	488021.028	2732556.728	-21.193	1	00:05.2	FLMK	0.008	0.013	Concrete Corner
AT042A	491421.856	2733276.321	-20.851	1	00:05.8	FLMK	0.009	0.013	Stop Bar
AT042B	491422.032	2733275.757	-20.843	1	00:05.8	FLMK	0.008	0.012	Stop Bar
AT042C	491427.567	2733278.335	-20.827	1	0:00:05	FLMK	0.009	0.013	Stop Bar
AT042D	491427.436	2733277.644	-20.827	1	00:05.8	FLMK	0.008	0.013	Stop Bar
AT043A	491853.809	2731032.681	-21.536	1	0:00:05	FLMK	0.010	0.015	Stop Bar
AT043B	491854.155	2731032.127	-21.536	1	0:00:05	FLMK	0.010	0.016	Stop Bar
AT043C	491851.148	2731029.925	-21.469	1	0:00:05	FLMK	0.010	0.016	Stop Bar
AT043D	491851.576	2731029.514	-21.482	1	00:05.6	FLMK	0.010	0.015	Stop Bar
AT044A	496181.251	2735363.509	-21.815	1	0:00:05	FLMK	0.005	0.010	Stop Bar
AT044B	496180.739	2735363.287	-21.824	1	0:00:05	FLMK	0.005	0.012	Stop Bar
AT044C	496179.408	2735368.708	-21.674	1	0:00:05	FLMK	0.007	0.012	Stop Bar

PID	Easting (m)	Northing (m)	Ellipsoid Height (m)	Occ. Count	Avg. Session Length	Ref. Base	Horiz. RMSE (m)	Vert. RMSE (m)	Target Type
AT044D	496178.872	2735368.486	-21.671	1	00:05.2	FLMK	0.007	0.012	Stop Bar
AT045A	498082.491	2734096.913	-21.458	1	0:00:05	FLMK	0.005	0.010	Arrow
AT045B	498081.363	2734097.519	-21.446	1	00:05.6	FLMK	0.005	0.010	Arrow
AT045C	498080.670	2734096.405	-21.451	1	0:00:05	FLMK	0.005	0.010	Arrow
AT046A	499091.910	2735793.192	-21.568	1	0:00:05	FLMK	0.007	0.013	Diamond
AT046B	499089.885	2735792.285	-21.544	1	0:00:05	FLMK	0.007	0.012	Diamond
AT046C	499090.712	2735793.118	-21.549	1	0:00:05	FLMK	0.007	0.012	Diamond
AT046D	499090.995	2735792.411	-21.559	1	0:00:05	FLMK	0.007	0.012	Diamond
AT047A	494613.771	2734322.287	-20.990	1	0:00:05	FLMK	0.004	0.007	Stop Bar
AT047B	494613.814	2734322.956	-20.996	1	00:05.8	FLMK	0.005	0.009	Stop Bar
AT047C	494610.522	2734321.520	-20.976	1	0:00:05	FLMK	0.006	0.010	Stop Bar
AT047D	494610.539	2734320.907	-20.983	1	0:00:05	FLMK	0.006	0.010	Stop Bar
AT048A	502338.496	2737154.289	-21.278	1	0:00:05	FLMK	0.008	0.015	Stop Bar
AT048B	502338.727	2737153.730	-21.238	1	0:00:05	FLMK	0.008	0.015	Stop Bar
AT049A	504263.177	2738883.165	-21.216	1	0:00:05	FLMK	0.009	0.019	Stop Bar
AT049B	504263.434	2738882.598	-21.225	1	0:00:05	FLMK	0.009	0.019	Stop Bar
AT049C	504260.399	2738880.754	-21.106	1	0:00:08	FLMK	0.008	0.020	Stop Bar
AT049D	504260.789	2738880.299	-21.087	1	0:00:05	FLMK	0.009	0.019	Stop Bar
AT050A	505724.418	2739282.386	-21.375	1	00:05.8	FLMK	0.009	0.019	Arrow
AT050B	505725.357	2739281.947	-21.322	1	0:00:05	FLMK	0.009	0.019	Arrow
AT050C	505725.144	2739282.969	-21.374	1	0:00:05	FLMK	0.009	0.019	Arrow
AT051A	511213.684	2741632.660	-19.642	1	0:00:05	FLMK	0.010	0.017	Arrow
AT051B	511212.924	2741631.992	-19.613	1	00:05.8	FLMK	0.010	0.017	Arrow
AT051C	511213.931	2741632.005	-19.589	1	00:05.8	FLMK	0.010	0.017	Arrow
AT052A	515309.828	2743236.392	-19.533	1	00:05.6	FLMK	0.011	0.020	Arrow
AT052B	515310.600	2743237.018	-19.532	1	00:05.8	FLMK	0.011	0.019	Arrow
AT052C	515309.596	2743237.047	-19.495	1	0:00:05	FLMK	0.011	0.019	Arrow
AT053A	518881.072	2745727.430	-22.035	1	0:00:05	FLMA	0.010	0.015	Arrow
AT053B	518881.704	2745729.040	-22.005	1	0:00:05	FLMA	0.010	0.015	Arrow
AT053C	518882.722	2745727.709	-22.053	1	0:00:05	FLMA	0.010	0.015	Arrow
AT054A	520987.069	2747230.607	-21.171	1	0:00:05	FLMA	0.010	0.018	Stop Bar
AT054B	520982.354	2747228.592	-21.296	1	0:00:05	FLMA	0.010	0.018	Stop Bar
AT054C	520982.106	2747229.112	-21.344	1	0:00:05	FLMA	0.010	0.017	Stop Bar
AT054D	520986.836	2747231.158	-21.193	1	0:00:05	FLMA	0.010	0.017	Stop Bar
AT055A	524418.537	2747109.796	-20.269	1	0:00:05	FLMA	0.013	0.018	Arrow
AT055B	524419.168	2747110.558	-20.299	1	0:00:05	FLMA	0.012	0.018	Arrow
AT055C	524419.501	2747110.065	-20.287	1	0:00:05	FLMA	0.012	0.018	Arrow
AT056A	527266.525	2749012.389	-22.158	1	0:00:05	FLMA	0.011	0.015	Stop Bar
AT056B	527268.473	2749009.515	-22.203	1	0:00:05	FLMA	0.011	0.015	Stop Bar
AT056C	527267.986	2749009.180	-22.198	1	0:00:05	FLMA	0.011	0.015	Stop Bar

PID	Easting (m)	Northing (m)	Ellipsoid Height (m)	Occ. Count	Avg. Session Length	Ref. Base	Horiz. RMSE (m)	Vert. RMSE (m)	Target Type
AT056D	527266.029	2749012.039	-22.140	1	0:00:05	FLMA	0.011	0.016	Stop Bar
AT057A	531037.878	2751847.952	-21.835	1	0:00:05	FLMA	0.011	0.019	Stop Bar
AT057B	531039.493	2751845.179	-21.812	1	0:00:05	FLMA	0.011	0.019	Stop Bar
AT057C	531038.980	2751844.876	-21.827	1	0:00:05	FLMA	0.011	0.019	Stop Bar
AT057D	531037.408	2751847.691	-21.830	1	0:00:05	FLMA	0.011	0.019	Stop Bar
AT058A	535236.890	2754384.758	-20.439	1	0:00:05	FLPK	0.009	0.017	Stop Bar
AT058B	535236.598	2754385.312	-20.425	1	0:00:05	FLPK	0.009	0.017	Stop Bar
AT058C	535230.773	2754379.760	-20.411	1	00:05.2	FLPK	0.009	0.016	Stop Bar
AT058D	535231.193	2754379.327	-20.432	1	0:00:05	FLPK	0.009	0.017	Stop Bar
AT059A	538923.948	2757929.187	-22.341	1	0:00:05	FLPK	0.008	0.012	Stop Bar
AT059B	538924.409	2757928.762	-22.329	1	00:05.4	FLPK	0.007	0.013	Stop Bar
AT059C	538927.957	2757932.380	-22.315	1	0:00:05	FLPK	0.008	0.013	Stop Bar
AT060A	543992.452	2761010.140	-21.709	1	0:00:05	FLPK	0.008	0.010	Stop Bar
AT060B	543991.981	2761010.463	-21.723	1	0:00:05	FLPK	0.008	0.010	Stop Bar
AT060C	543988.866	2761006.373	-21.760	1	0:00:05	FLPK	0.008	0.010	Stop Bar
AT060D	543989.201	2761005.844	-21.771	1	0:00:05	FLPK	0.008	0.010	Stop Bar
AT061A	546788.164	2765208.771	-22.484	1	0:00:05	FLPK	0.008	0.015	Arrow
AT061B	546787.189	2765209.681	-22.501	1	0:00:05	FLPK	0.008	0.013	Arrow
AT061C	546785.918	2765208.575	-22.492	1	0:00:05	FLPK	0.008	0.013	Arrow
AT062A	550878.841	2769448.588	-21.427	1	00:05.8	FLPK	0.007	0.015	Stop Bar
AT062B	550879.463	2769448.565	-21.443	1	0:00:05	FLPK	0.008	0.015	Stop Bar
AT062C	550879.467	2769452.035	-21.466	1	00:05.2	FLPK	0.008	0.016	Stop Bar
AT063A	555159.791	2774322.003	-21.075	1	00:57.2	FLPK	0.009	0.020	Stop Bar
AT063B	555159.956	2774321.437	-21.028	1	0:00:23	FLPK	0.009	0.020	Stop Bar
AT063C	555163.695	2774324.870	-21.015	1	00:21.2	FLPK	0.009	0.020	Stop Bar
AT063D	555163.306	2774325.339	-21.008	1	0:00:17	FLPK	0.009	0.020	Stop Bar
AT064A	559233.005	2779029.067	-20.785	1	0:00:05	FLPK	0.011	0.018	Stop Bar
AT064B	559236.493	2779034.847	-20.727	1	00:36.4	FLPK	0.012	0.020	Stop Bar
AT064C	559237.077	2779034.644	-20.765	1	00:09.2	FLPK	0.012	0.019	Stop Bar
AT064D	559232.491	2779029.395	-20.811	1	00:08.8	FLPK	0.012	0.020	Stop Bar
AT065A	562953.258	2784213.879	-23.923	1	00:21.2	FLPK	0.010	0.020	Stop Bar
AT065B	562952.652	2784213.891	-23.939	1	0:00:09	FLPK	0.010	0.020	Stop Bar
AT065C	562952.721	2784217.212	-23.930	1	0:00:22	FLPK	0.010	0.019	Stop Bar
AT065D	562953.315	2784217.189	-23.914	1	0:00:07	FLPK	0.010	0.020	Stop Bar
AT066_	560892.389	2785999.701	-22.675	1	0:00:08	HMST	0.011	0.020	Cross
AT066A	558058.543	2788406.195	-23.522	1	0:00:05	FLPK	0.008	0.016	Stop Bar
AT066B	558060.685	2788400.292	-23.438	1	0:00:05	FLPK	0.008	0.015	Stop Bar
AT067A	569194.015	2793623.220	-22.355	1	0:00:06	HOME	0.011	0.018	Stop Bar
AT068A	564929.575	2786386.694	-22.669	1	00:26.2	FLPK	0.009	0.018	Arrow
AT068B	564929.232	2786385.798	-22.668	1	00:05.2	FLPK	0.009	0.018	Arrow

PID	Easting (m)	Northing (m)	Ellipsoid Height (m)	Occ. Count	Avg. Session Length	Ref. Base	Horiz. RMSE (m)	Vert. RMSE (m)	Target Type
AT068C	564928.774	2786386.163	-22.618	1	0:00:05	FLPK	0.009	0.018	Arrow
AT069A	571016.362	2799226.034	-23.027	1	0:00:07	HOME	0.011	0.019	Stop Bar
AT069B	571016.087	2799226.647	-23.019	1	00:06.2	HOME	0.011	0.019	Stop Bar
AT069C	571020.105	2799227.612	-23.087	1	0:00:32	HOME	0.012	0.020	Stop Bar
AT069D	571019.874	2799228.177	-23.066	1	00:05.2	HOME	0.011	0.019	Stop Bar
AT070A	584546.439	2840596.234	-24.155	1	00:05.2	FLMB	0.010	0.018	Cross
AT070B	584546.692	2840598.044	-24.156	1	0:00:05	FLMB	0.010	0.017	Cross
AT070C	584546.408	2840598.042	-24.150	1	00:05.2	FLMB	0.010	0.017	Cross
AT070D	584544.661	2840596.478	-24.225	1	0:00:09	FLMB	0.010	0.016	Cross
AT070E	584544.652	2840596.173	-24.210	1	00:05.8	FLMB	0.010	0.016	Cross
AT070F	584546.224	2840594.435	-24.178	1	0:00:05	FLMB	0.010	0.016	Cross
AT070G	584546.493	2840594.429	-24.189	1	0:00:05	FLMB	0.010	0.016	Cross
AT070H	584548.247	2840596.017	-24.153	1	0:00:05	FLMB	0.010	0.016	Cross
AT070I	584548.266	2840596.312	-24.166	1	0:00:05	FLMB	0.010	0.016	Cross
AT071A	583618.379	2842648.479	-24.678	1	00:06.2	FLMB	0.012	0.019	Stop Bar
AT071B	583618.215	2842648.911	-24.672	1	00:05.8	FLMB	0.011	0.018	Stop Bar
AT071C	583622.387	2842650.384	-24.648	1	00:05.2	FLMB	0.010	0.018	Stop Bar
AT071D	583622.446	2842649.954	-24.624	1	0:00:05	FLMB	0.011	0.017	Stop Bar
AT072A	584811.733	2845532.280	-24.890	1	0:00:05	FLMB	0.010	0.015	Arrow
AT072B	584810.564	2845532.523	-24.938	1	0:00:05	FLMB	0.010	0.015	Arrow
AT072C	584810.823	2845531.423	-24.927	1	00:05.8	FLMB	0.012	0.017	Arrow
AT073A	583154.503	2847236.611	-24.483	1	00:05.2	FLMB	0.009	0.013	Arrow
AT073B	583153.766	2847235.744	-24.459	1	0:00:05	FLMB	0.009	0.012	Arrow
AT073C	583154.898	2847235.407	-24.481	1	0:00:05	FLMB	0.009	0.012	Arrow
AT074A	578972.119	2847352.732	-24.106	1	0:00:05	FLUM	0.007	0.018	Arrow
AT074B	578973.020	2847352.238	-24.087	1	0:00:05	FLUM	0.007	0.018	Arrow
AT074C	578972.268	2847351.716	-24.091	1	0:00:05	FLUM	0.007	0.013	Arrow
AT075A	586743.086	2850171.427	-24.109	1	0:00:05	FLMB	0.006	0.009	Arrow
AT075B	586744.112	2850171.491	-24.100	1	0:00:15	FLMB	0.010	0.016	Arrow
AT075C	586743.739	2850170.653	-24.107	1	0:00:05	FLMB	0.009	0.015	Arrow
AT076A	587449.588	2853412.176	-23.915	1	0:00:05	FLMB	0.010	0.014	Arrow
AT076B	587448.688	2853410.889	-23.928	1	0:00:05	FLMB	0.010	0.015	Arrow
AT076C	587448.174	2853411.648	-23.908	1	0:00:05	FLMB	0.009	0.014	Arrow
AT077A	587158.561	2855745.165	-24.999	1	0:00:05	FLMB	0.006	0.011	Arrow
AT077B	587157.797	2855746.055	-25.012	1	0:00:05	FLMB	0.006	0.011	Arrow
AT077C	587158.731	2855746.990	-25.020	1	0:00:05	FLMB	0.006	0.011	Arrow
AT078A	579905.011	2853706.561	-21.201	1	0:00:05	FLUM	0.007	0.017	Stop Bar
AT078B	579904.826	2853711.275	-21.287	1	0:00:05	FLUM	0.008	0.018	Stop Bar
AT078C	579906.217	2853710.841	-21.294	1	0:00:21	FLUM	0.009	0.020	Stop Bar
AT078D	579906.345	2853706.621	-21.244	1	0:00:05	FLUM	0.007	0.018	Stop Bar

PID	Easting (m)	Northing (m)	Ellipsoid Height (m)	Occ. Count	Avg. Session Length	Ref. Base	Horiz. RMSE (m)	Vert. RMSE (m)	Target Type
AT079A	580856.395	2857063.958	-21.649	1	0:00:05	FLMB	0.005	0.010	Crosswalk
AT079B	580857.617	2857063.997	-21.625	1	0:00:05	FLMB	0.006	0.012	Crosswalk
AT079C	580856.531	2857060.943	-21.672	1	0:00:05	FLMB	0.006	0.011	Crosswalk
AT079D	580857.728	2857060.999	-21.651	1	0:00:05	FLMB	0.006	0.011	Crosswalk
AT080A	583048.982	2855002.146	-24.529	1	0:00:05	FLMB	0.005	0.009	Concrete Corner
AT080B	583047.465	2855002.073	-24.555	1	0:00:05	FLMB	0.005	0.009	Concrete Corner
AT080C	583047.377	2855003.603	-24.547	1	0:00:05	FLMB	0.005	0.009	Concrete Corner
AT080D	583048.904	2855003.678	-24.534	1	0:00:05	FLMB	0.005	0.009	Concrete Corner
AT081	570171.952	2796826.481	-24.538	1	0:03:00	HMST	0.007	0.015	Cross
AT082	460781.891	2734811.917	-20.998	1	0:03:00	FLMK	0.008	0.011	Cross
QA001A	418398.461	2715513.056	-19.611	1	0:00:05	FLKW*	0.010	0.015	Crosswalk
QA001B	418398.453	2715513.368	-19.633	1	0:00:05	FLKW*	0.011	0.016	Crosswalk
QA001C	418397.928	2715513.328	-19.623	1	0:00:05	FLKW*	0.011	0.016	Crosswalk
QA001D	418397.921	2715513.631	-19.590	1	0:00:05	FLKW*	0.011	0.016	Crosswalk
QA001E	418395.500	2715512.880	-19.623	1	0:00:05	FLKW*	0.012	0.018	Crosswalk
QA001F	418395.457	2715513.465	-19.593	1	0:00:05	FLKW*	0.013	0.018	Crosswalk
QA002	498192.296	2735415.189	-21.447	1	0:00:05	FLMA	0.007	0.011	Arrow
QA003A	428328.335	2718539.263	-19.337	1	0:00:05	FLKW*	0.008	0.017	Crosswalk
QA003B	428324.976	2718541.391	-19.364	1	0:00:05	FLKW*	0.007	0.015	Crosswalk
QA003C	428344.565	2718554.783	-19.423	1	0:00:05	FLKW*	0.007	0.015	Crosswalk
QA004	508570.851	2739689.264	-22.194	1	0:00:05	FLMA	0.010	0.016	Stop Bar
QA005A	445717.798	2722896.519	-21.036	1	0:00:05	FLKW	0.007	0.012	Stop Bar
QA005B	445717.415	2722897.001	-21.032	1	0:00:05	FLKW	0.007	0.013	Stop Bar
QA005C	445713.635	2722893.218	-21.183	1	0:00:05	FLKW	0.007	0.013	Stop Bar
QA006	463533.254	2724498.742	-21.158	1	0:00:05	FLKW*	0.007	0.013	Chevron
QA007A	489406.383	2732720.721	-21.286	1	0:00:05	FLMK	0.005	0.009	Stop Bar
QA007B	489406.342	2732721.332	-21.297	1	0:00:05	FLMK	0.005	0.009	Stop Bar
QA007C	489412.366	2732721.915	-21.243	1	0:00:05	FLMK	0.005	0.009	Stop Bar
QA007D	489412.413	2732721.304	-21.254	1	0:00:05	FLMK	0.005	0.009	Stop Bar
QA008	463839.261	2728541.704	-20.639	1	0:00:05	FLKW*	0.009	0.015	Stop Bar
QA010	529038.240	2749981.008	-22.554	1	0:00:07	FLMA	0.010	0.020	Diamond
QA011	582402.346	2852321.819	-23.793	1	0:00:05	FLUM	0.006	0.010	Arrow
QA012	557734.847	2776994.095	-21.327	1	0:00:10	HMST	0.011	0.019	Arrow
QA013	584689.170	2843808.612	-24.716	1	0:00:05	FLUM	0.008	0.012	Arrow
QA014	565237.052	2786788.481	-22.639	1	0:00:05	HMST	0.012	0.019	Arrow
QA015A	465735.557	2727945.514	-21.590	1	0:00:15	FLMK	0.011	0.019	Stop Bar
QA015B	465734.991	2727945.544	-21.592	1	0:00:15	FLMK	0.011	0.018	Stop Bar
QA015C	465734.980	2727942.495	-21.632	1	0:00:15	FLMK	0.011	0.018	Stop Bar
QA015D	465735.572	2727942.461	-21.644	1	0:00:15	FLMK	0.011	0.019	Stop Bar

* See Table 17 for information about the Reference Bases and FLKW.

Aerotriangulation Report

FL1806 Florida Keys Topo-Bathy Project

July 2019

Area Covered

The project area centers around and encompasses the entire Florida Keys area, including all its constituent islands from the Miami metropolitan area at its northeastern end to just beyond Dry Tortugas National Park at its southwestern end. The AOI covers approximately 2,135 square miles and approximately 1,991 miles of shoreline. The AOI curves around the southeastern and southern tip of the Florida peninsula, running almost 180 miles from Miami in the northeast to beyond Key West in the southwest. For its northern two-thirds, the AOI is roughly 7-10 miles wide as it follows the curve of the Keys towards the south and southwest. Just west of Marathon, FL and Boot Key, however, the AOI flares out sharply to the north-northwest to be 20 miles wide, gradually narrowing back down to a little over 13 miles wide at its southwestern terminus just to the west of the Dry Tortugas. This "flare out" covers a very large area of shallows and uninhabited islands around and to the north of Little Pine Key, Howe Key, Big Torch Key, including most of the Great White Heron National Wildlife Refuge, as well as much of the Key West National Wildlife Refuge. The east and southeast edge of the AOI encompasses much of the Hawk Channel, the John Pennekamp Coral Reef State Park, and Biscayne National Park. The AOI includes all of the primary Florida Keys within Monroe County, Florida (Key Largo to Key West), as well as a small portion of Miami-Dade County extending in a 7 to 10 mile-wide strip from Old Rhodes Key north to include the MacArthur Causeway, South Beach, and a small portion of downtown Miami itself). The project is located approximately between 24°26'17" and 25°47'52" North Latitude, and 80°05'02" and 82°13'19" West Longitude.

Imagery

The photography used in the aerotriangulation phase was flown by Geomni and consisted of thirty-eight (38) flight lines, and one thousand three hundred forty (1340) 4Band color photographs. The photographs were acquired at a nominal ground sample distance of 0.33 meters using the DMCII 230-526 camera with a 92.00 mm lens. The 4band color photographs were acquired by Geomni on January 8, 10, and 17. February 17 and 18. April 21, 23, and May 20 of 2019. All imagery was acquired using >60% forward overlap and >30% side overlap, sun angles >20 or >25 degrees (depending on the date of acquisition) and was coordinated with low tide. The layout of the photographs is shown in the attached diagrams. Photographic coverage, resolution, overlap, and metric quality were adequate for the performance of the aerotriangulation phase.

Control

A combination of photo identifiable ground control points and Airborne GPS/IMU data were used to control the imagery for aerotriangulation.

A. Airborne GPS/IMU: Airborne GPS and IMU data were collected and processed by Geomni and provided to Quantum Spatial via external hard drive. ABGPS exposure stations were used as control in the aerotriangulation, and inertial measuring unit (IMU) measurements were used to refine these.

B. Ground Points: QSI was dispatched to survey two hundred fifty-seven (257) photo ID control points (horizontal and vertical), thirty-three (33) points were added for vertical accuracy using NOAAs 2014 LIDAR, and 4 check points. Four surveyed points were used to check the horizontal and vertical accuracy of the aerotriangulation. The results of the survey have been published in the final ground control report that has been included in this Aerotriangulation submission to NGS.

Overall, the ground control points were found to be adequate to supplement the airborne GPS control.

Methodology

The photographs were bridged using digital aerotriangulation methods to establish the network of photogrammetric control required for the compilation phase. The images were bridged in a bundle adjustment that included all 1340 4Band color non-tide coordinated images. Measurements were made utilizing a digital photogrammetric workstation running the Windows 10 operating system. Hexagon's ImageStation Automatic Triangulation (ISAT) software was used to perform automatic point measurements and interactive point measurements of tie points. The final adjustment of the block was accomplished by using a rigorous simultaneous least squares bundle adjustment, and analysis tools within ISAT were used to refine the aerotriangulation solution and to evaluate the accuracy of the adjustment.

Analysis of Results

The final ISAT results were evaluated for the triangulation adjustment providing a display of the image and point residuals and connections between frames. Weak points and blunders were identified and corrected. The final aerotriangulation solution for the image block was computed in ISAT as a full bundle block adjustment. The RMS of the standard deviations in both X and Y directions were calculated and used to determine the radius of the 95% confidence circle for each image block. The predicted horizontal circular error accuracy (RMSE or 95% CI) is 0.37m for the 4band photos. (see Annex 3 for details of the computations). This accuracy refers to the overall block, but in the bundle adjustments the error was distributed such that the largest errors are associated with points around the edges of the project and areas of vast water where the strength of the solution is weakest, while points down the middle of each block located on areas of extensive land cover have the smallest errors because those points are measured on a greater number of images. In addition, each of the four (4) ground control check points measured in and the coordinates and elevations of these check points were not constrained at all in any of the block adjustments, but were treated as pass points, and adjusted coordinates were computed, and the differences are shown below:

4Band

POINT ID	ΔX M	ΔY M	ΔZ M
AT005C	-0.093	-0.006	0.022
AT047A	0.072	-0.162	0.190
AT065D	0.200	-0.097	0.350
AT073B	0.174	-0.025	0.448

As a final check select models from each strip of photography were examined in DAT/EM Summit Evolution to ensure the horizontal and vertical integrity of the ISAT 2015 solution, and to verify the suitability of the database for use in the compilation phase. The images were checked for proper parallax, ground control tolerance, and check point tolerance. Models covering the four check points referenced above were specifically reviewed in this manner, and included the following:

Point ID	Flight Lines & Images	Image Dates
AT005C	120023 120023_0011, 120023_0012	2-17-2019
AT047A	120003 120003_0009, 120003_0010	1-17-2019
AT065D	120010 120010_0024, 120010_0025	1-08-2019
AT073B	120016 120016_0019, 120016_0020	1-10-2019

To conclude, the aerotriangulation block meets the horizontal standards set forth by NOAA in Chapter I of the Version 14A Statement of Work for Shoreline Mapping.

Project Deliverables

The following files have been included in this submittal.

- o Exposure Stations
- o Electronic Exposure Data (EED)
- o Camera calibration data
- o Ground Control File
- o Ground Control Report
- o Airborne GPS Control File and IMU Orientation Original DG
- o Adjusted Exterior Orientation parameters for each frame
- o RGB/NIR Stereo Imagery
- o RGB/NIR Stereo Imagery Metadata
- o Flight Line and Frame Shapefile
- o Airborne Positioning and Orientation Report (APOR)
- o Tabulation of Aerial Photography
- o AT Report

Positional data is based on the North American Datum of 1983 (NAD83 (2011) and is referenced to the Universal Transverse Mercator (UTM) Zone 17 coordinate system.
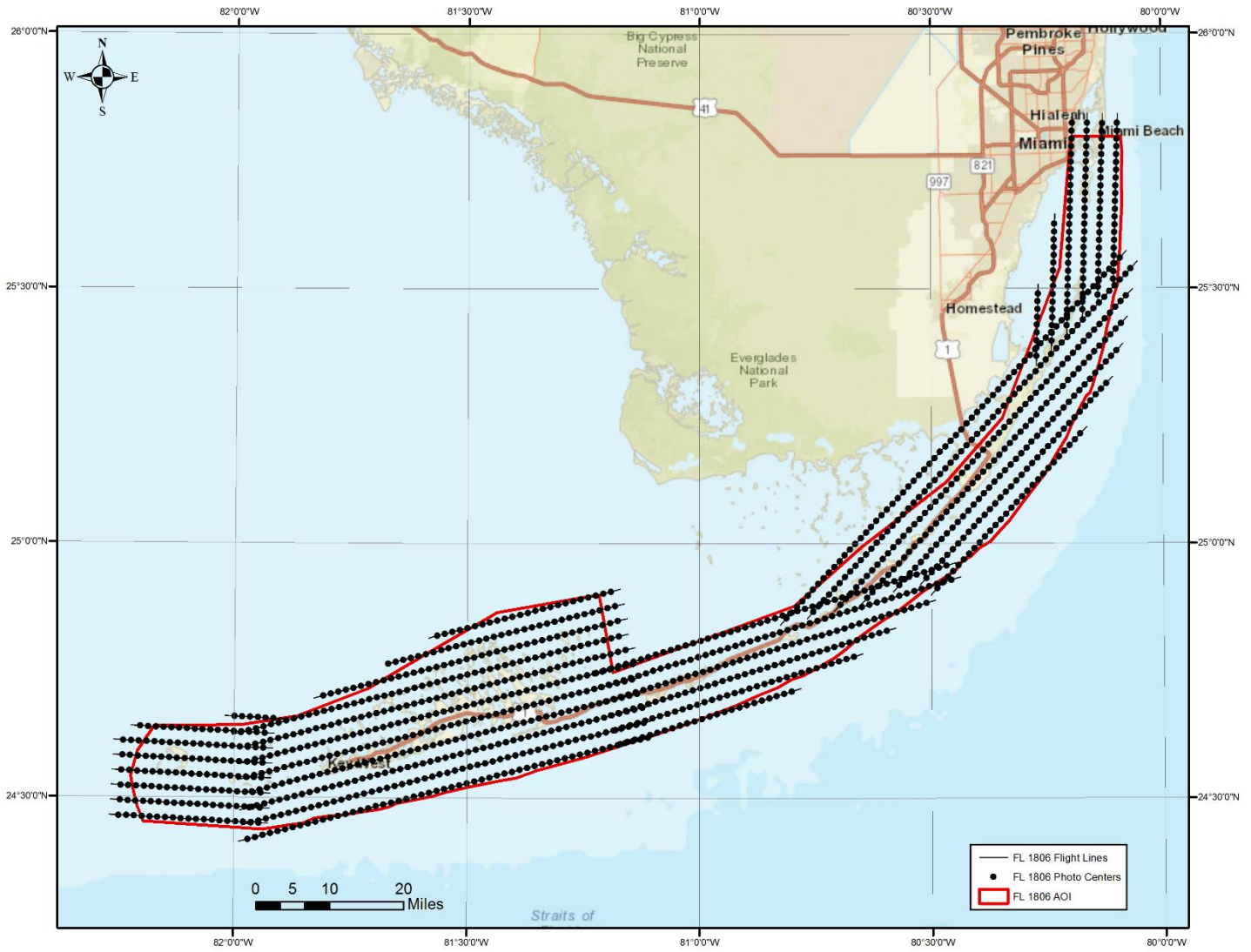
ANNEX 1 – Project Location

Project Location Diagram
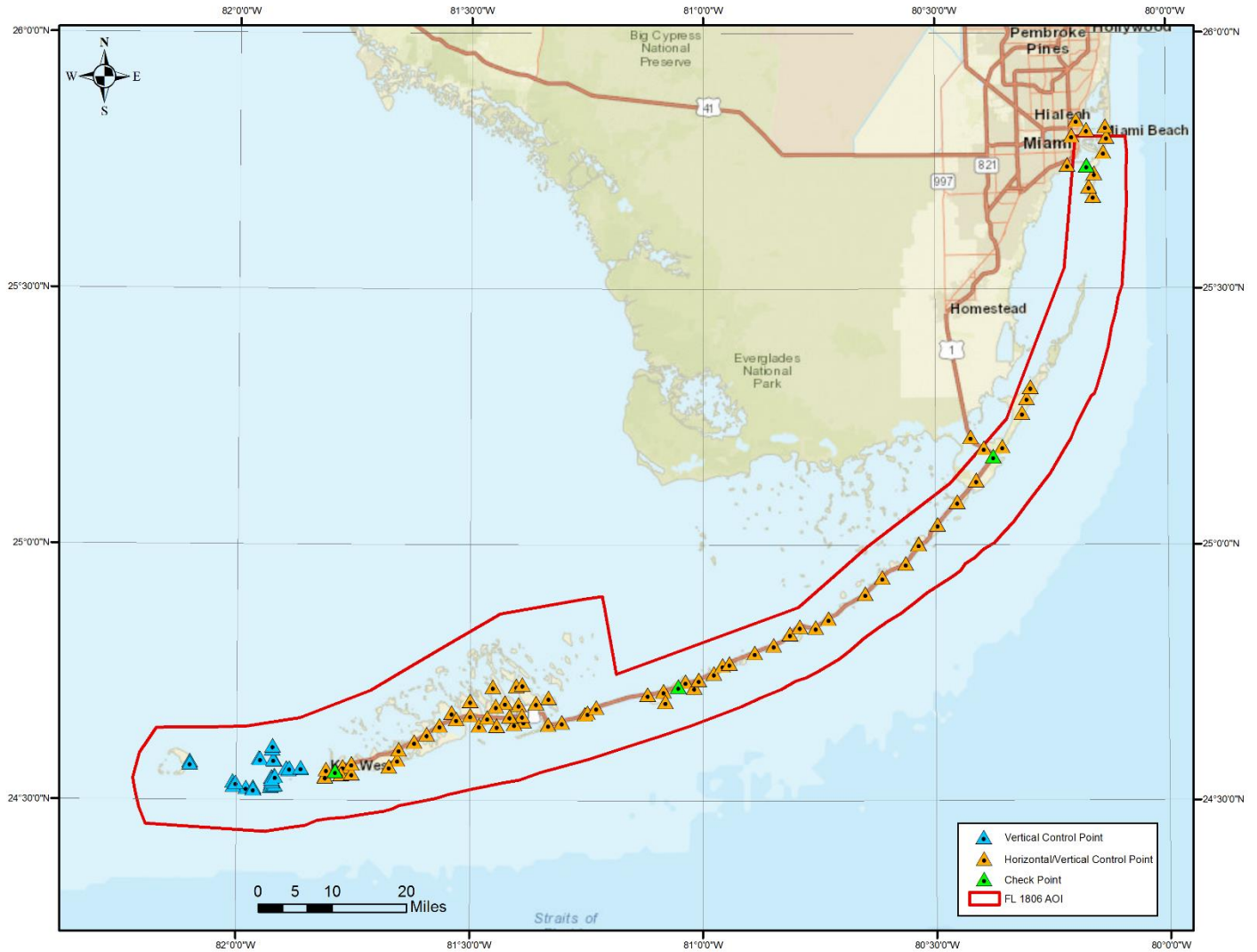
ANNEX 2A – 4Band – Flight Lines

Flight Line Diagram – 4 Band

FL1806

ANNEX 2B – 4Band– Flight Line Table

Flight Line ID	Starting Image ID	Ending Image ID	Date Flown
120001	120001_0024	120001_0001	1/17/2019
120002	120002_0001	120002_0033	1/17/219
120003	120003_0101	120003_0108	1/17/2019
120003	120003_0009	120003_0038	1/17/2019
120004	120004_0044	120004_0001	1/17/2019
120005	120005_0001	120005_0048	1/17/2019
120006	120006_0048	120006_0001	1/17/2019
120007	120007_0028	120007_0001	1/8/2019
120008	120008_0001	120008_0035	1/8/2019
120009	120009_0042	120009_0001	1/8/2019
120010	120010_0001	120010_0049	1/8/2019
120011	120011_0055	120011_0001	1/8/2019
120012	120012_0001	120012_0061	1/8/2019
120013	120013_0001	120013_0064	1/17/2019
120014	120014_0021	120014_0001	1/10/2019
120015	120015_0001	120015_0023	1/10/2019
120016	120016_0025	120016_0001	1/10/2019
120017	120017_0001	120017_0027	1/17/2019
120018	120018_0016	120018_0001	1/17/2019
120019	120019_0009	120019_0001	1/17/2019
120020	120020_0054	120020_0001	2/17/2019
120021	120021_0001	120021_0053	2/17/2019
120022	120022_0053	120022_0001	2/17/2019
120023	120023_0001	120023_0052	2/17/2019

120024	120024_0052	120024_0001	2/17/2019
120025	120025_0001	120025_0052	2/17/2019
120026	120026_0051	120026_0033	2/17/2019
120026	120026_0015	120026_0032	5/20/2019
120026	120026_0014	120026_0001	2/17/2019
120027	120027_0001	120027_0036	2/17/2019
120027	120027_0137	120027_0145	4/21/2019
120028	120028_0001	120028_0040	4/23/2019
120029	120029_0123	120029_0101	4/23/2019
120030	120030_0024	120030_0001	4/21/2019
120031	120031_0019	120031_0001	2/18/2019
120032	120032_0001	120032_0019	2/18/2019
120033	120033_0019	120003_0001	2/18/2019
120034	120034_0001	120034_0009	2/18/2019
120034	120034_0110	120034_0117	2/18/2019
120035	120035_0019	120035_0001	5/20/2019
120036	120036_0001	120036_0019	5/20/2019
120037	120037_0017	120037_0001	5/20/2019
120038	120038_0006	120038_0001	5/20/2019

ANNEX 3 - Horizontal Accuracy Computation

The Horizontal Accuracy Statement reported in the Analysis of Results is based on the predicted circular horizontal accuracy of adjusted points in the aerotriangulation solution. This circular accuracy equals the radius of the 95% confidence circle as calculated from the horizontal (x and y) root-mean-square (RMS) values of the standard deviations for all triangulated ground points, rounded to the nearest tenth of a meter.

The root mean square of all standard deviations of triangulated ground points:

Block 1 (NC)   RMS(x) =0.074 meters   RMS(y) =0.076 meters

The value for the confidence circle radius is given by the following expression:

R=K*Sx

Where Sx is defined as the larger of the two (X and Y) RMS values, and K is interpolated using the C ratio from the Table of Cumulative Probability.

The C ratio equals the smaller of the RMS values divided by the larger:

Block 1 (NC):   C=0.074/0.076=0.97

The following line (95% probability level) from the Table of Cumulative Probability was used to determine the value of K by a simple linear interpolation between the two nearest values of C:

C	0	.1	.2	.3	.4	.5	.6	.7	.8	.9	1.0
K(95%)	1.95996	1.96253	1.97041	1.98420	2.00514	2.03586	2.08130	2.14598	2.23029	2.33180	2.44775

Block 1 (NC)

    K   =2.33180 + [(.97 -0.9) / (1.0-0.9) * (2.44775 - 2.3318)]

          =2.33180 + (0.7 * 0.11595)

          =2.33180 + .0.081165

    K   =2.37818 =2.41724

    R   = K * Sx = 2.41724 * 0.076 = .183

The Radius of the 95% Confidence Circle 0.183 **meters**